EINDHOVEN UNIVERSITY OF TECHNOLOGY

Eindhoven University of Technology

MASTER

Secondary electron emission of MgO films

van Gogh, A.T.M.

Award date:
1995

Link to publication

Disclaimer
This document contains a student thesis (bachelor's or master's), as authored by a student at Eindhoven University of Technology. Student theses are made available in the TU/e repository upon obtaining the required degree. The grade received is not published on the document as presented in the repository. The required complexity or quality of research of student theses may vary by program, and the required minimum study period may vary in duration.

General rights
Copyright and moral rights for the publications made accessible in the public portal are retained by the authors and/or other copyright owners and it is a condition of accessing publications that users recognise and abide by the legal requirements associated with these rights.

- Users may download and print one copy of any publication from the public portal for the purpose of private study or research.
- You may not further distribute the material or use it for any profit-making activity or commercial gain

Secondary Electron Emission of MgO films

by A.T.M. van Gogh

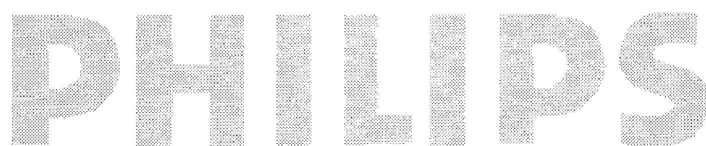

Report of the work done from January until December 1995 at the 'Natuurkundig Laboratorium' in Eindhoven, part of the research division of Philips Electronics NV.

Supervisors: dr. J.J. Scholtz (Philips)
Prof. dr. H.H. Brongersma (Technical University Eindhoven)

Eindhoven, December 1995.

Abstract

In this work the secondary electron emission (SEE) properties of in situ grown MgO films and the influence of charging effects on these properties are studied. The necessary experimental set-up was built and improved.

From experiments on wedge-shaped layers a maximum secondary emission yield δ_{max} of 24 for monocrystalline and 16 for polycrystalline MgO was found. The higher value for monocrystalline MgO is found to be due to a greater secondary electron escape depth in monocrystalline MgO. The escape depth was found to be approximately 20 nm for polycrystalline MgO and 75 nm for monocrystalline MgO.

For both poly- and monocrystalline MgO a first cross-over energy E_I of 15 eV was measured, independent of the film thickness in the range from 5 to at least 50 nm. The intrinsic SEE properties of MgO were found to be independent of the crystal face and the substrate. The measure of charging and therefore the effects of this on the secondary electron emission do depend on these parameters, as well as on the film thickness and the primary beam current distribution.

From numerical simulations it was found, that the typical features, which are observed on the δ-curves of insulators at low primary energies, can be inderstood by the influence of an inhomogeneous surface potential distribution. Possible effects arising from a divergence of the electron beam do not play a role of importance.

Measurements showed that up to a certain value of the primary current, the core potential of the surface potential distribution is independent of the sign of the sample potential V_A during the electron bombardment. However, the surface potential distribution in the outer area seems to flatten when $V_A<0$ V during the electron bombardment. For higher beam currents, the core potential starts to rise in case $V_A<0$ V, while it remains unaltered when $V_A>0$ V.

The most consistent explanation of the observed increase of the SEE of MgO in successive measurements is secondary electron field enhancement, caused by an induced space charge in the interior of the film.

Table of Contents

Abstract

Chapter 1: Introduction **1**

Chapter 2: Theory **3**

§2.1 Secondary Electron Emission 3
§2.1.1 Understanding the phenomenon 5
§2.1.2 SEE, a semi-empirical model 6
§2.2 Charging and conduction mechanisms 8

Chapter 3: Experiments **12**

§3.1 Measuring $\delta(E_p)$ 12
§3.2 Building the set-up 17
§3.3 Sample Preparation 20

Chapter 4: Results **22**

§4.1 SEE at high primary energies ($E_p \gtrsim 100$ eV) 22
§4.2 SEE at low primary energies ($E_p \lesssim E_1$) 28
§4.2.1 $\delta(E_p \lesssim E_1)$ of MgO films 28
§4.2.2 Arteficial effects 31
§4.3 Surface Potential Measurements 43
§4.4 SEE Enhancement 51

Chapter 5: Conclusions **57**

References **60**

Dankwoord **61**

Appendix: MgO Data Table

Chapter 1: Introduction

When the surface of a material is bombarded with electrons, other electrons can be released. When these so-called secondary electrons are emitted from the material one speaks of secondary electron emission (SEE). The secondary electron emission yield δ is defined as

$$\delta \doteq \frac{i_s}{i_p}, \qquad (1.1)$$

in which the primary current i_p is the electron current incident on the surface. The secondary current i_s is the total current of secondary electrons leaving the material's surface.
Many parameters play a role in determining the SEE properties of a specific material. Important parameters are for example the physical density, conductivity, workfunction, or in case of a semiconductor or insulator the sum of the bandgap and electron affinity, crystallinity, surface morphology. Also of influence on δ are the in- or external electrical fields.
When the material under consideration is insulating, a δ which differs from one will result in sample charging. It is obvious that this will influence the SEE properties of the material, because charging of the bulk and surface will change its electromagnetic properties and therefore its interaction with the primary and secondary electrons. For example, charging of the sample's surface will alter E_p. So in case of an insulating sample, additional parameters, which influence the charging properties of the sample, are also important. Parameters one can think of in this case are sample thickness, primary current density j_p and crystallinity.

The phenomenon of SEE was discovered in 1902 by Austin and Starke [1]. At first only little interest was shown, but when electronic tubes came into more general use, the phenomenon was also more intensively studied. Since then SEE has been the subject of numerous investigations.
The importance of electronic tubes in contemporary technology has diminished, but there are still some important applications of SEE as there are the scanning electron microscope (SEM), electron multipliers and magnetron tubes. Understanding of the phenomenon is also important for solving problems involving SEE in for example plasma displays and cathode ray tubes.
For most practical applications, materials with a high SEE are of interest, because it makes multiplication of electrons possible. Materials with a low SEE can be used as electron absorbers.
From a more scientific point of view SEE is interesting, because of its complexity. As mentioned before, there are a lot of parameters which have to be dealt with. One has to describe a many particle problem in which free electrons enter a solid and in case of insulators one has to reckon with charging phenomena which may change the material properties during the electron bombardment. Additionally, time dependent effects occur under some conditions.
Since long MgO has been an interesting material for studying SEE. Like many other insulating metal oxides it is characterized by a high maximum secondary

emission yield δ_{max}. Values of δ_{max} have been reported of 20 to 25 as well on single crystals cleaved under vacuum conditions [2] as on thin crystalline films [3]. Other reasons why MgO is interesting from a technical point of view is that it is stable under electron bombardment and relatively cheap. From a more scientific point of view MgO is interesting as a *model* because of its simple cubic structure (fcc) and its insulating properties.

During this work SEE properties of *in situ* grown MgO films were investigated. It was the first time that this was done at this laboratory. In the past only *ex situ* grown MgO films were studied. The necessary experimental set-up was built. With this set-up, measurements of δ as a function of the kinetic energy E_p of the primary electrons, Auger electron spectroscopy (AES) and LEED can be done.
The parameters, of which the influence was studied are film thickness, j_p, electrical field geometry, substrate properties, crystallinity and crystal orientation in order to give more insight into the mechanism of SEE and charging phenomena.

To get a feeling for the parameters which play a role in determining the SEE properties of a certain material, a theoretical contemplation about SEE will be given in chapter 2 and also a semi-empirical model is discussed. In this chapter charging effects and conduction mechanisms are discussed as well.
In the third chapter will be explained how the secondary electron emission is measured. A summary is given of the problems which arose and the artefacts which were discovered during building of the set-up. The chapter also contains the procedures for film preparation.
The results of the measurements will be presented and discussed in the fourth chapter and in the last chapter a summary of the most important results and some recommendations for future experiments are given.

Chapter 2: Theory

§2.1 Secondary Electron Emission

The secondary emission yield δ, defined in (1.1) depends on the energy E_p of the primary electrons. A characteristic plot of δ versus E_p is shown in figure 2.1(a). Important parameters characterizing the SEE properties of a material are also shown. The maximum secondary electron yield is δ_{max} and the matching primary energy is referred to as E_{max}. The primary energies E_1 and E_2 are the first and second cross-over energies respectively. These are the primary energies for which δ=1. For crystalline MgO E_1 =10-20 eV and δ_{max} =20-25. The value of E_2 is of the order of 10 keV.

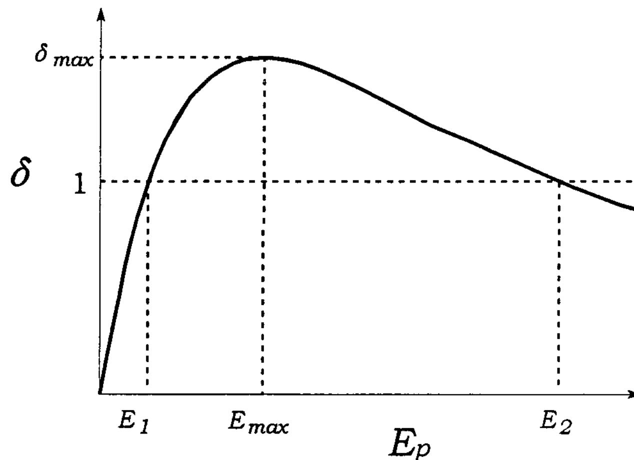

(a)

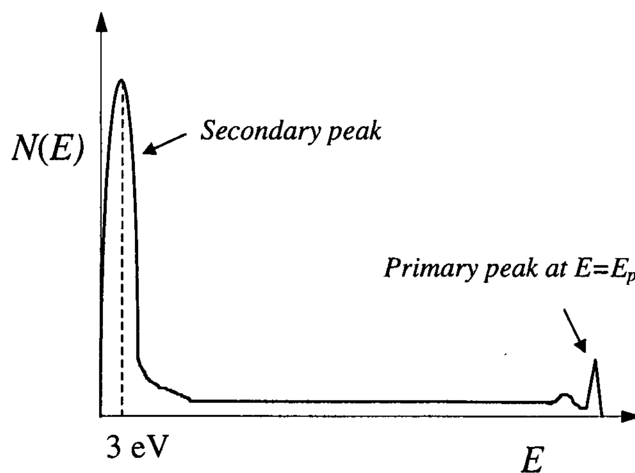

(b)

*-**Figure 2.1**- Secondary electron emission yield δ as a function of the primary energy (a) and the kinetic energy distribution of the secondary electrons (b).*

The maximum in the so-called δ-*curve* can be explained by the fact that at low E_p an increasing primary energy, increases the number of generated secondary electrons. At higher energies the depth at which secondary electrons are released starts to play a role. When the inelastic mean free path of the primary electrons becomes greater than the escape depth of the secondary electrons, a decrease in δ will be observed. For metals, the escape depth of the secondary electrons is typically 5 nm. For insulators the escape depth can be much greater. For example Bronshteyn and Brozdnichenko [4] find an escape depth of 5 nm for magnesium, while for magnesium oxide an escape depth of 32 nm is found. Borisov and Lepeshinskaya [5] found an even greater escape depth for MgO, namely 60 nm. The penetration depth for E_p=1-2 keV is approximately 40-100 nm.

The kinetic energy distribution of the secondary electrons is shown in figure 2.1(b). Most secondary electrons have an energy smaller than 10 eV. The low kinetic energy of the secondary electrons is due to multiple inelastic scattering processes, in which secondary electrons can produce new secondary electrons. This mechanism is called the *cascade effect*. Measurements showed, that the shape of the secondary peak is independent of E_p in the energy range between 20 and, at least, 3000 eV.
The above considerations do not explain the absence of very slow secondary electrons, or, in other words, do not explain the maximum in the energy distribution at low energies. This maximum is assumed as being due to internal reflection of very slow electrons at the surface. It is well known from quantum mechanics that electrons approaching a potential barrier, for example an MgO-vacuum interface, have a certain probability of being reflected. This internal reflection probability of the electrons at the surface increases with decreasing energy. The high surface potential barrier of metals in comparison with insulators, $\phi=\mathbf{O}(5\ \text{eV})$ while $\chi=\mathbf{O}(1\ \text{eV})$, is the reason that in general for metals the maximum in the energy distribution is situated a few electronvolts higher than in case of insulators [6].
It has to be emphasized that the explanations above are rather qualitative and that a thorough understanding of the *N(E)* distribution is much more complex.

As mentioned before, secondary electrons are the electrons which are released within the material by the impinging primaries and are emitted from the surface. In practice a distinction between these *real* secondary electrons and the elastically and inelastically reflected *primary* electrons, cannot be made off course. In some works, with *secondary electrons* are meant the electrons with an energy smaller than 50 eV, but this is not entirely correct, because the electrons with an energy between 50 eV and the primary energy consist of both inelastically reflected primaries and real secondary electrons and on the other hand, primary electrons can lose so much energy that they end up with an energy smaller than 50 eV.
In this work secondary electrons are defined as all the electrons which come from the material due to the electron bombardment.

§2.1.1 Understanding the phenomenon

When an electron enters the solid there is a certain probability that it will scatter. The statistical quantity characterizing this probability is the cross section σ, which is related to the mean free path λ (m.f.p.) by definition as $\sigma=1/N\lambda$, in which N is the total amount of scattering centers per m^2. The m.f.p. can be interpreted as the average distance which an electron travels, before it scatters. One distinguishes the *elastic* m.f.p. and the *inelastic* m.f.p. of electrons which scatter elastically or inelastically respectively.
Primary electrons can be *elastically* scattered by lattice atoms. A second mechanism is reflection of the primary electrons by the surface potential barrier. Although for incoming electrons this is not a barrier, the potential energy increases, a fraction of the primary electrons is still reflected. This effect is a well known and purely quantum mechanical effect.

Most secondary electrons are created by direct excitation of valence electrons to the conduction band. When $E_p \geq E_g-\chi$, an electron can excite a valence elctron to the conduction band. At lower energies ($E_p \leq E_g-\chi$), the inelastic effects are mainly due to electron phonon collisions. Valence electrons can also be excited indirectly by the decay of plasmons, excited by primary electrons.
Secondary electrons can also be created by excitation of core electrons. It is noted however that the core electrons give only a small contribution to the total amount of secondary electrons, because of the deep lying states from which they are excited.

In case of an insulator, the creation of secondary electrons will induce a certain space charge in the interior of the sample, which is positive when $\delta>1$. This will induce an electrical field in the film, which will cause a *Fowler-Nordheim tunneling* of electrons from the substrate into the conduction band of the insulator. The electrical field will rise until current continuity is established. If this field is sufficiently high, a fraction of the injected electrons will be emitted into the vacuum. This current thus represents a field enhanced component of the secondary electron emission. It is clear that this contribution to the secondary emission depends on the band structure of the substrate.
The induced electrical field also lowers the thermal activation energy of trapped electrons (polarons). This is called the *Poole-Frenkel effect.* The electrons which are released as a result of this effect contribute to the secondary current as well.

For metals the escape depth of secondary electrons is approximately 5 nm. In case of an insulator the escape depth is greater. One reason for this is that the secondary electrons can hardly be scattered by conduction electrons. A greater escape depth in general means a higher secondary emission yield, because more secondary electrons are able to reach the surface. This is one of the reasons why in general insulators have a higher δ. Lattice defects and impurities lower the escape depth and therefore δ.

It is hardly possible to understand SEE quantitatively from a microscopic point of view. The primary electrons will scatter more than once in most cases and their trajectories depend on the trajectories of the other primaries and created secondaries. One has to do with a typical example of a many particle problem, in which a more statistical approach is demanded. Nowadays good results can be achieved in solving these problems with Monte-Carlo simulations [7],[8].
A fraction of the reflected primary electrons will have been scattered once though and one may expect to see some structure in the energy distribution of the secondary electrons. This structure should be best visible near the elastic peak in the $N(E)$ distribution, because there will be few real secondary electrons with such a large energy. The analysis of matter in this way is called electron loss spectroscopy (ELS). The peaks which in general are best visible in such spectra are loss peaks due to the excitation of surface plasmons, but the fine structure in these spectra contains a lot more information about loss transitions in a certain material. An elegant study of secondary electron emission mechanisms in BaO in which EELS is used was done by Thomas et al [9]. The structure which they measure on the secondary peak of monocrystalline films is assigned to regions with a high density of states.

In the past, several theories were developed to describe secondary electron emission. Some are based on a model, either classical or quantum mechanical, others are more or less phenomenological. There is no theory which describes the whole phenomenon satisfactorily. In the next section however, a semi-empirical model obtained by Dionne [10],[11] is discussed, which gives insight in the mechanisms which are involved in the excitation of secondary electrons and which helps to understand the influence of certain parameters which are of importance for the SEE of MgO.

§2.1.2 SEE, a semi-empirical model

The model described by Dionne [10] is derived by doing the following assumptions.

1. The number of secondary electrons, produced by the primary electrons at a depth z in the material, is proportional to the energy loss per unit path length (dE/dz) of the primary electrons, divided by the energy ζ which is needed to produce an excited electron.
2. dE/dz is given by the *power law*: $dE/dz=-A/E^{n-1}$, in which A is the primary electron absorption constant. From experiments n=1.3-1.6.
3. The probability of an excited electron to reach the surface is proportional to $\exp(-\alpha z)$, in which α is a secondary electron absorption coefficient.
4. The effective escape probability of an electron which has reached the surface is equal to B.
5. The scattering of the primary electrons is included by assuming that the average energy loss of the primary electrons is independent of the penetration depth z: $dE/dz=-E_p/\lambda_p$, in which λ_p is the maximum penetration depth of the primary electrons.

For the secondary emission yield is then found

$$\delta = \frac{B}{\zeta}\left(\frac{An}{\alpha}\right)^{1/n}\left(\alpha\lambda_p\right)^{\frac{1}{n}-1}(1-e^{-\alpha\lambda_p}). \tag{2.2}$$

By setting $\partial\delta/\partial(\alpha\lambda_p)=0$ and n=1.35 in [11] the following expressions for δ_{max} and E_{max} are derived

$$\delta_{max} = 0.9\left(\frac{B}{\zeta}\right)\left(\frac{A}{\alpha}\right)^{0.74},$$
$$E_{max} = 2.3\left(\frac{A}{\alpha}\right)^{0.74}. \tag{2.3}$$

By setting δ=1 and assuming $\alpha\lambda_p$<<1, which is correct when δ_{max}>2.5, the following expression for E_1 is derived:

$$E_1 \approx \frac{\zeta}{B}. \tag{2.4}$$

In the same work a similar expression is derived for E_2. However, in this work not much attention is paid to the second cross-over energy. Therefore the expression is not given here.

It is recalled that A is the primary electron absorption constant. In other words it represents the *stopping power* of the solid and should therefore be directly proportional to the physical density.
By definition, α is an inverse mean free path, which is determined by the electrical conductivity. Metals should therefore have large values of α and insulators small ones. Since α is reasonably uniform among metals and among insulators, it is likely that A will control the ratio A/α .
The parameter B is the escape probability for electrons at the top of the potential barrier. As was mentioned in section 2.1, in general this probability is higher for insulators.
In case of a metal, ζ represents the workfunction ϕ and the sum of the band gap E_g and the electron affinity χ for an insulator or semiconductor. For metals $\phi=\mathbf{O}(5\text{ eV})$, while $E_g+\chi=\mathbf{O}(10\text{ eV})$ for insulators. For MgO E_g=7.8 eV and χ=0.85 eV as can be found in the MgO data table (see Appendix).

From the above, it is concluded that the maximum yield is depends directly on the physical density and inversely on the conductivity and $E_g+\chi$ (or the workfunction in case of a metal). It is known that E_g greatly influences the conductivity by an exponential function. It is therefore not unlikely that the negative effect of a higher conductivity on δ_{max}, because of a smaller value of E_g, dominates the positive effect on δ_{max} by the decrease of ζ. This could be the reason why insulators with large band gaps have high yields.
E_{max} is fully determined by A/α. A and α are bulk parameters and are therefore independent of the physical condition of the surface. This explains the

experimental result that E_{max} is hardly affected by surface contamination. On the other hand E_1 is fully determined by ζ/B. This can be understood by the fact that in general $E_{max}>>E_1$. Therefore the mean depth at which the secondary electrons are generated at $E_p=E_{max}$ is much greater than at $E_p=E_1$.
It is easy to understand that δ_{max} depends both on surface as on bulk properties. The bulk properties determine the amount of secondary electrons which are released within the material and the surface properties determine the amount of secondary electrons which can leave the material.
It is not known how B will vary with different adsorbates. In case of ζ, it is well known that metal work functions are affected by adsorption of various substances and that the electron affinities of insulators and semiconductors may vary greatly with monolayers of adsorbate. In some cases, for alkali-metal oxides, the value of χ is believed to become negative. Under these conditions, extremely high values of δ have been observed [12]. Borisov and Lepeshinskaya [5] found in case of MgO that δ can be raised to high values, by reducing the surface barrier, through the deposition of thin Cs or Li films on the MgO surface. On the other hand, a carbon surface contamination reduces δ.

§2.2 Charging and conduction mechanisms

Figure 3.1 shows that in the used measuring method, a cathode is used, which emits electrons by heating of a filament. This cathode has a negative potential V_C with respect to earth. The part of the electron gun where the electrons leave is grounded at zero potential, so the kinetic energy of the electrons leaving the gun is equal to $|e \cdot V_C|$. The potential V_G of the first grid which is surrounding the sample is also 0 V. The potential V_A of the anode, or in fact the sampleholder, is varied from the cathode potential to 0 V to set the primary energy of the electrons. For this primary energy then the following relation holds:

$$E_p = e \cdot (V_A + V_S) - e \cdot V_C, \qquad (2.1)$$

in which e is the elementary charge and V_S the surface potential.
For this cathode-grid-film system there are four stable values for V_S, which the surface of an insulating film can reach during electron bombardment.
Suppose in the next four cases that initially $V_S=0$ V. The sample is biased negatively with respect to the grid to set a certain E_p. Initially the secondary electrons will then be pushed away from the surface towards the grid.

First suppose that the surface is initially bombarded with electrons with $E_p<E_1$. In this case $\delta<1$ and the surface will therefore be negatively charged. Consequently the primary electrons will be retarded and will impinge on the surface with a smaller kinetic energy. This process continues until no primary electrons are able to reach the surface anymore. At that moment V_S has reached a stable value equal to $V_C - V_A$. This process is visualized by curve 1 in figure 2.2. Because of the condition $E_p < E_1$, the value of V_A has to be smaller than $V_C + E_1/e$. For the final value of V_S then holds $V_S = V_C - V_A \geq E_1/e$.

Secondly suppose that the surface is bombarded with electrons with $E_1<E_p<E_2$. Because the surface charges positively, the primary energy of the next incoming electrons increases. As a consequence, the surface will charge positively more and more until V_S becomes so high that $E_p=E_2$. In that case $\delta=1$, no further charging will occur and V_S will remain constant at $E_2\,/e+(V_C-V_A)$, see curve 2 in figure 2.2.

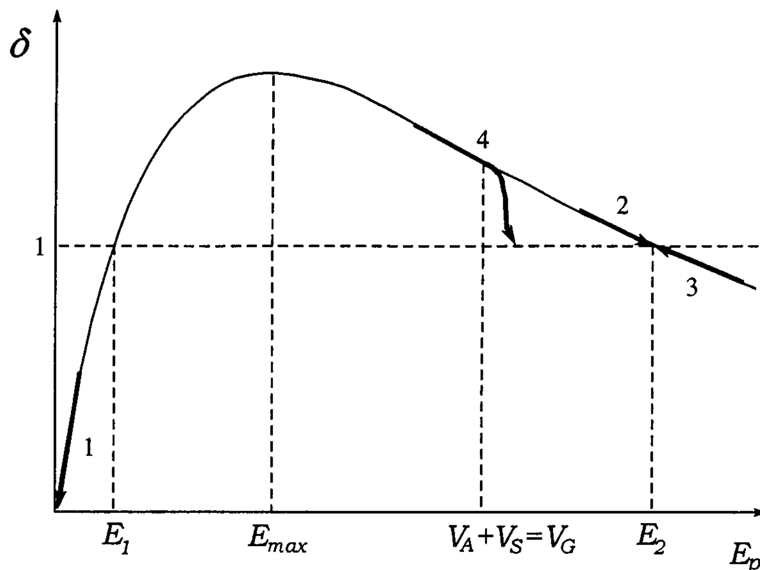

-Figure 2.2- *Visualization of the charging mechanisms for an ideal insulator as described in the text, using an intrinsic δ-curve.*

The third stable situation is reached when one starts with $E_p>E_2$. The surface charges negatively and the incoming electrons will be retarded. This process will continue until E_p equals E_2 . No further charging will occur, V_S remains constant and is equal to $E_2\,/e+(V_C-V_A)$ This process is visualized by curve 3 in figure 2.2.

The last stable situation is reached when one starts with $E_p>E_1$ and when $e\cdot(V_G-V_C)<E_2$, which will be always the case in this work. The surface will charge positively until V_S becomes so high that V_A+V_S equals V_G. When in that case the surface potential increases further, secondary electrons will be pulled back to the sample and as a consequence, δ will collapse and reach an equilibrium value of 1. In this stable situation, V_A+V_S has reached a value typically a few volts higher than V_G (curve 4 in figure 2.2). For the surface potential now holds $V_S=-V_A$ plus a few volts. The value of the final surface potential is thus determined by the initial value of V_A.
Notice that when the condition $e\cdot(V_G-V_C)<E_2$ is not satisfied, E_p will reach E_2 before V_A+V_S reaches V_G and the third instead of the last stable situation will be established.

The situation $E_p=E_1$ is unstable. An infinitesimal *positive* charging will finally establish the second or fourth stable situation, while an infinitesimal *negative* charging will establish the first stable situation.

The considerations above are equivalent to that of Seggern [13] and of Bruining [6] (p 19-21).

To understand the influence of an increase of the primary current and film thickness, the MgO layer is considered as a capacitor, with an area A equal to the area of the electron beam and a thickness d of the dielectric equal to the film thickness.
The increase of the potential ΔV_S as a consequence of the deposited charge Q in a time interval Δt at the point where the electron beam hits the surface is given by

$$\Delta V_S = \frac{Q}{C} = \frac{i_p \Delta t d}{\varepsilon_0 \varepsilon_r A}. \tag{2.2}$$

In (2.2) C is the capacity, for which is used

$$C = \frac{\varepsilon_0 \varepsilon_r A}{d}, \tag{2.3}$$

with $\varepsilon_0\ \varepsilon_r$ being the dielectric constant. It is clear that both an increase of i_p and the sample thickness, increase the induced potential.

The charging mechanisms described above, hold for a perfect insulator and in case of homogeneous charging of the surface. In real insulating materials there will always be some conduction, which will diminish the effects described above. Moreover the surface charge will not be distributed homogeneously over the surface.

When describing the *conduction* of electrons in thin films one has to reckon with two contributions. The first contribution is the conduction through the bulk. Note that it is not likely that the conduction of secondary electrons and primary electrons through film can be described by an Ohmic law. This law describes the transport of conduction electrons under the influence of an applied electrical field and may therefore not be applied to *hot electrons*. Cazaux et al. [14] observed a current transport through an insulating MgO film, which was orders of magnitude higher than could be expected from Ohm's law.
The second contribution is conduction along the surface of the film by the so-called *hop transport* of secondary electrons. This transport can take place in the presence of an electrical field along the surface and an electrical field perpendicular to the surface, which pulls back secondary electrons which leave the surface. When in addition the kinetic energy of the secondary electrons which hit the surface again is approximately equal to E_1, it can be shown that a certain feed back mechanism is established, which keeps the average value of E_p, with which the electrons hit the surface, equal to E_1. Therefore the secondary electrons which are pulled back to the surface generate an equal amount of new secondary electrons, because $\delta(E_1) = = 1$. Before these electrons hit the surface again, they will

have travelled a certain distance along the surface, due to the component of the electrical field along the surface, resulting in a net electron current along the surface.

It is found that it is possible that secondary electrons are pulled back to the surface, while $V_A+V_S<0$ V [15],[16]. It was mentioned before that this is only possible for $V_A+V_S>0$ V. This subtle effect is caused by an inhomogeneous charging of the surface. A small positive value of V_S creates a potential barrier near the surface of the sample. Although in general this potential barrier is very small compared to V_A, secondary electrons may not be able to overcome this barrier because of their low kinetic energy. This effect is visualized in figure 2.3.

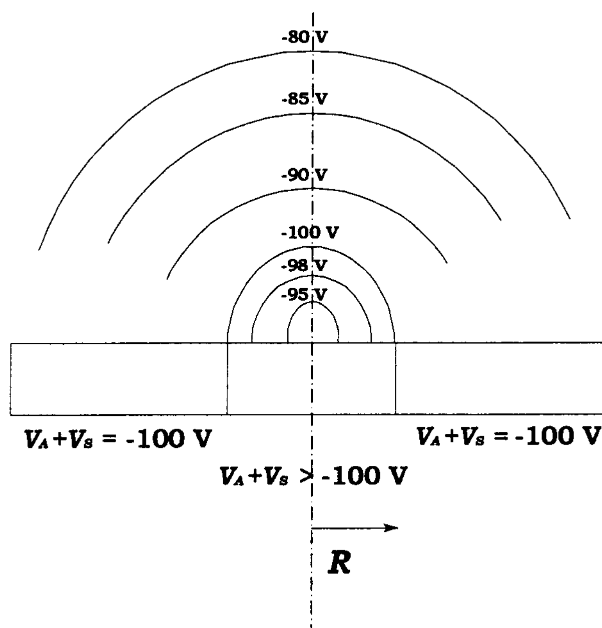

-Figure 2.3- *Due to a local positive charging of the surface with respect to the surrounding area, a potential barrier can be created, which pulls back secondary electrons, while* $V_A+V_S<V_G$.

Chapter 3: Experiments

§3.1 Measuring $\delta(E_p)$

The SEE measurements were carried out under ultra high vacuum conditions ($p \lesssim 10^{-9}$ Torr). A schematic overview of the measuring method is given in figure 3.1. A four grids Omicron Spectaleed set-up was used as electron gun and as an earthed shield surrounding the sample under consideration.

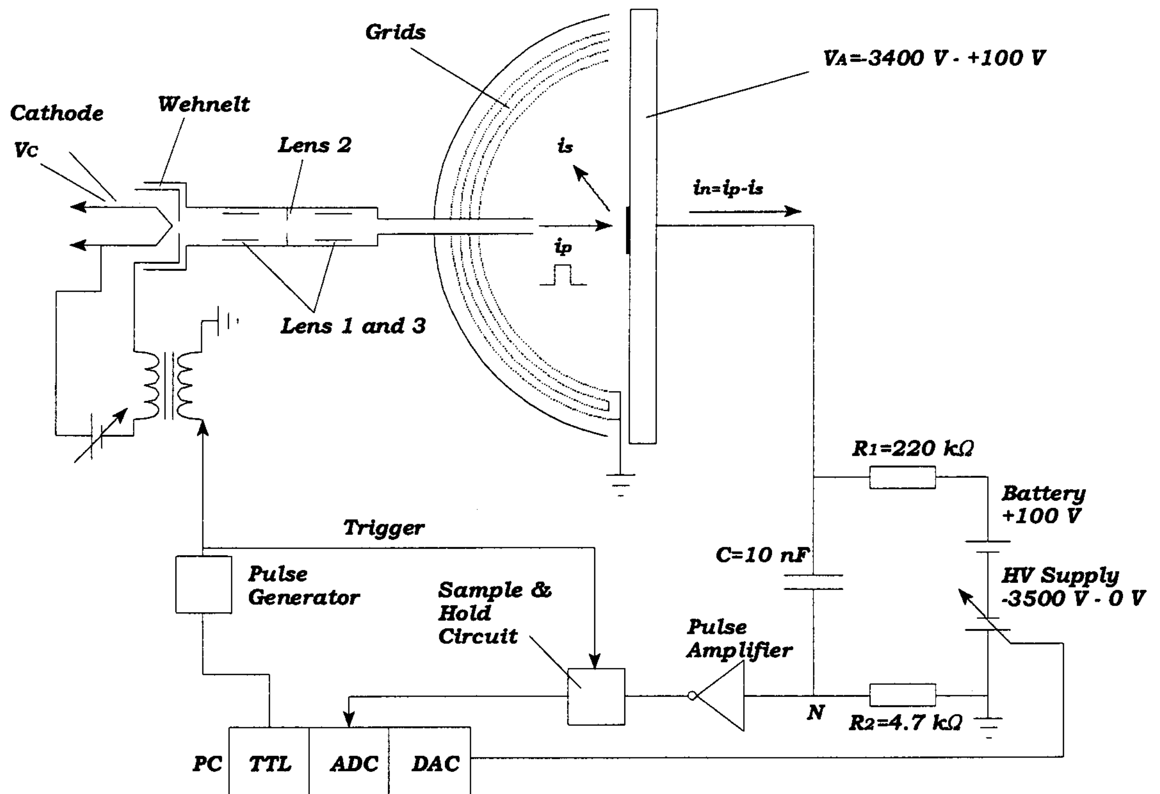

*-**Figure 3.1**- Schematic overview of the set-up for measuring $\delta(E_p)$.*

Two gun supplies were used, namely an Omicron 1 kV NGL-10 and an Omicron 3.5 kV NGE-35 gun supply.
The pulse amplifier in figure 3.1 is a Canberra research amplifier, model 1412. At first an EG&G Ortec spectroscopy amplifier model 570 was used, but the Canberra has more extensive shaping time possibilities with which it is possible to achieve a better signal to noise ratio. Another advantage of this amplifier is that it has the possibility to amplify a 5 μs pulse without distortion. This is of importance for

experiments considering the Malter effect (see page 56), which are to be done in the future.
Two high voltage (HV) supplies were used during the experiments. For measurements with $E_{gun} \leq 3.5$ keV a FUG HCN 14-3500 3.5 kV supply was used. For measurements with $E_{gun} \leq 1.4$ keV a PHI auger system control, model 11-500-A was used, which was modified to make it possible to control it externally with a PC. Its maximum output voltage was 1.5 kV. The PHI power supply gives less noise than the FUG, so more accurate measurements can be done with it.
The value of δ is determined by measuring the current i_n , which flows to earth via the sample and by measuring the primary current i_p .

$$\delta \doteq \frac{i_s}{i_p} = \frac{i_p - i_n}{i_s} = 1 - \frac{i_n}{i_p}. \tag{3.1}$$

The currents which contribute to i_n are:

1. Surface current caused by hop transport,
2. Current through the sample,
3. Displacement current. In case of a perfectly insulating sample only a displacement current is measured. The sample can be considered as a capacitor.

The primary energy of the electrons leaving the gun E_{gun} is kept constant. By varying V_A from 0 V to $-E_{gun}/e$ the primary energy of the electrons is set from E_{gun} to 0 eV. This method has two advantages.
First the negative bias on the sampleholder will diminish charging problems. When the surface of the sample is charged positively with respect to the sampleholder and when this charge is homogeneously distributed over the surface, no electrons are pulled back to the surface, because in most cases the surface is still biased negatively with respect to the grid.
A second advantage is that E_{gun} can be kept constant during a measurement of $\delta(E_p)$. This means that i_p has to be measured only once. If E_p is set by varying E_{gun}, i_p has to be measured for every value of E_p, because i_p depends strongly on E_{gun}.

In order to keep the charging of the sample as small as possible, the surface is bombarded with short pulses of electrons. This is done by pulsing the wehnelt cylinder of the electron gun. The pulse duration is 5 μs and in most measurements $i_p = \mathbf{O}(10^{-11}$ C/pulse).

When i_n is a square shaped pulse with an amplitude i_m and a pulse duration Δt, the potential V_p at point N in figure 3.1 as a function of time is given by

$$V_p = i_m \frac{R_1 R_2}{R_1 + R_2} e^{-\frac{t}{C(R_1+R_2)}}, \tag{3.2}$$

for $0<t<\Delta t$.

For $t>\Delta t$, V_p is given by

$$V_p = -i_m \frac{R_1 R_2}{R_1 + R_2}\left[1 - e^{-\frac{t}{C(R_1+R_2)}}\right] e^{-\frac{t-\Delta t}{C(R_1+R_2)}}. \quad (3.3)$$

Because $C(R_1+R_2)$=2.25 ms which is very long compared to 5 μs, the pulse at point N can be considered as square shaped with an amplitude proportional to i_m. After amplification this pulse is measured with a sample and hold circuit.

The primary current is measured by setting the power supply to 0 V, so V_A becomes +100 V. In that case $E_p = E_{gun} + 100$ eV= E_{tot}. In this case for i_n holds

$$i_n = i_p - i_s \int_{100eV}^{E_{tot}} N(E)dE = i_p - i_p \delta(E_{tot}) \int_{100eV}^{E_{tot}} N(E)dE = i_p(1-\alpha) \approx i_p, \quad (3.4)$$

in which (3.1) is used and α is defined as

$$\alpha \doteq \delta(E_{tot}) \int_{100eV}^{E_{tot}} N(E)dE. \quad (3.5)$$

The approximation made in (3.4) is only valid under the condition $\alpha \ll 1$.
The measured δ, called δ' is related to the intrinsic δ via

$$\delta' = \frac{\delta - \alpha}{1 - \alpha}. \quad (3.6)$$

In this work α was measured as a function of E_{gun}. The result is given in figure 3.2. When E_{gun} is equal to 1,2 or 3 keV, α=0.15, 0.08 or 0.04 respectively. For δ' then holds:

1. $\delta'(E_p; E_{gun}= 1\text{ keV}) = 1.18\cdot(\delta(E_p)-0.15)$; $\delta=10 \Rightarrow \delta'=11.62$,
2. $\delta'(E_p; E_{gun}= 2\text{ keV}) = 1.09\cdot(\delta(E_p)-0.08)$; $\delta=10 \Rightarrow \delta'=10.81$,
3. $\delta'(E_p; E_{gun}= 3\text{ keV}) = 1.04\cdot(\delta(E_p)-0.04)$; $\delta=10 \Rightarrow \delta'=10.36$.

It follows from (3.6) that when $\delta=1$, also $\delta'=1$. When however $\delta<1$ and $\alpha<1$ the measured value of δ is smaller than the intrinsic δ, while in case $\delta>1$ and $\alpha<1$, δ' is higher than the intrinsic δ.
So the right value for E_1 is measured, but for δ_{max} the measured value is too high.

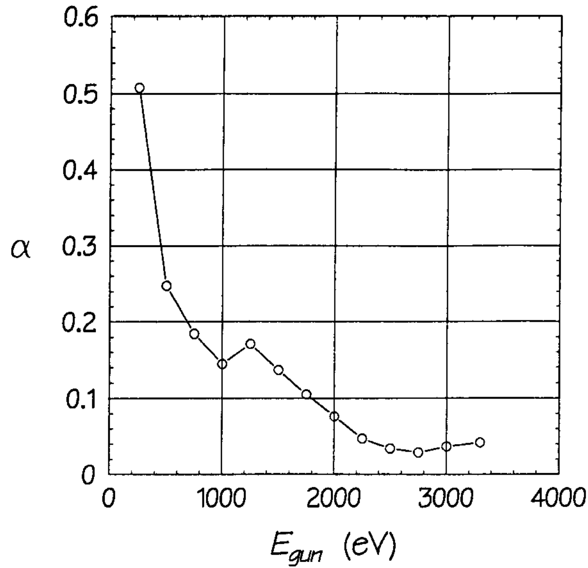

*-**Figure 3.2**- α as a function of E_{gun}. The error made in δ becomes smaller for smaller values of α. Thus for E_{gun}≈2.8 keV, δ' approximates δ best.*

In case of an insulating sample, negative charging will influence the measurement of i_p. Because of V_A =+100 V, most secondary electrons will be pulled back to the surface. Therefore a certain surface potential distribution is created. Hendriks [15] calculated how this distribution will look like (Figure 3.3).

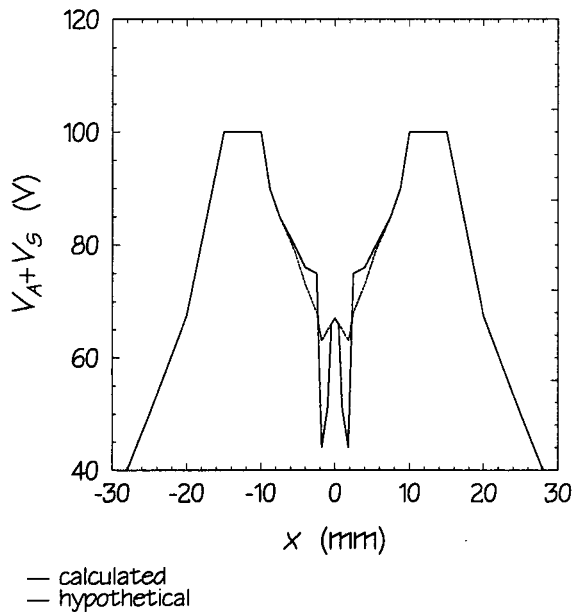

*-**Figure 3.3**- The result of a Monte-Carlo simulation of the potential distribution over the sample, which is created by the measurement of i_p. The potential of the sampleholder is +100 V. Due to the hop transport the potential of the whole sample is lowered with respect to the sample holder. The electron beam lands with R=0.5 mm symmetrically around **x=0** on the sample. The sample width is 20 mm and that of the sampleholder 30 mm. The hypothetical potential distribution is discussed in §4.4.*

When there is no leaking current, i_s will become equal to i_p. As a consequence a zero primary current will be measured, because of i_n=0. However, the created electrical field along the surface acts as a transport field, which enables electrons to hop over the surface to the sampleholder. This is the current, which is measured in the steady state. It is smaller than the real i_p, because reflected primary electrons do not contribute to this leaking current. This i_n in fact increases the value of α, but measurements of $\alpha(E_{gun})$ already showed that α is small enough for our purposes.

The whole measuring procedure of i_p and $\delta(E_p)$ is integrated in a computerprogram which sets E_p by setting V_A and measures i_n by reading out the sample and hold circuit via an ADC.

§3.2 Building the set-up

In the beginning of the work, the UHV system, the necessary electronics and a computerprogram for doing the measurements were available. During the installment of all the parts, several problems arose and were solved.

The first main problem which arose was to pulse the wehnelt cylinder of the electron gun. By loading the pulse generating circuit with the wehnelt cylinder, the pulse height collapsed. The origin of the problem was found in the parasitic capacity of the used coax cables. The problem was simply solved by connecting a capacitor parallel to the potentiometer setting the wehnelt voltage in order to decrease the RC-time of the circuit.
It is known that the primary current density j_p is an important parameter in SEE experiments on insulators, because of the charging effects. With this in mind, a study was made of the focussing properties of the used gun with attention to the spot size, diverging angle and spot profile of the electron beam. This was done by visual observation of the spot on a luminescensing sample of $CaWO_3$.

On δ-curves measured with a focussed beam a strange structure was observed (Figure 3.4). This lump in the δ-curve, visible at E_p =400 eV in the figure, was determined to be due to a second primary electron beam with a lower energy than the set E_{gun}. This second primary electron beam is generated by electrons which impinge on the first or third focussing lens, which are in fact electrostatic deflection plates and are set to the same potential. These electrons create secondary electrons which are accelerated by the negative voltage of the lens. The energy with which the electrons leave the gun is equal to the voltage V_{lens} of the lenses plus the energy of the secondary electrons which is in the order of a few eV (Figure 2.1(b)). This explanation was confirmed by making a spectrum of the electron beam using the RFA (Figure 3.5).

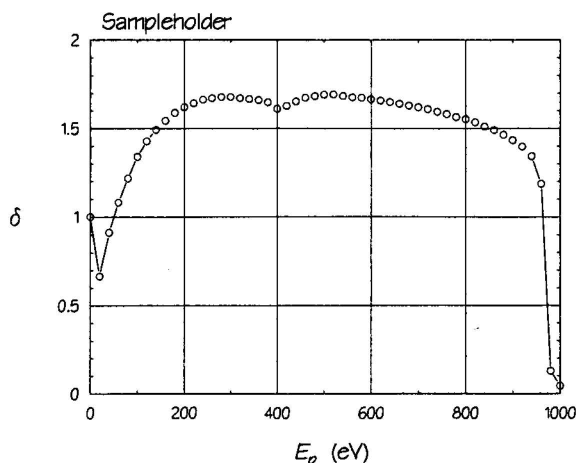

Figure 3.4- *δ-curve measured with a focussed electron beam. The hump at $E_p \approx 400$ eV is a second δ-curve caused by a second primary electron beam with an energy smaller than the set E_{gun}.*

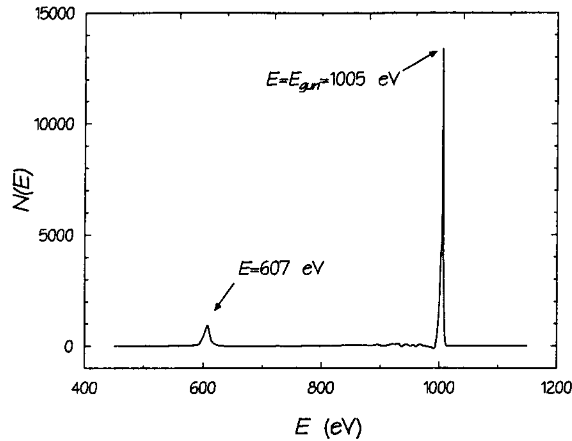

-***Figure 3.5***- *Energy spectrum of a focussed electron beam with V_{lens}=-600 V. The spectrum was made using the retarding field analyzer and by setting the sampleholder to a voltage lower than $-E_{gun}/e$, in order to reflect all the electrons coming from the gun.*

The energy of the secondary beam was measured to be equal to $e \cdot |V_{lens}| + \mathbf{O}(10\text{ eV}) \approx e \cdot |V_{lens}|$. During a measurement of a δ-curve the secondary beam can reach the sample when $|V_A| \leq |V_{lens}|$, and will then start with the creation of secondary electrons on the sample. This should occur as a second δ-curve upon the original δ-curve starting at $E_p = E_{gun} - e \cdot |V_{lens}|$, which was confirmed experimentally.
The problem was solved by setting V_{lens} to a voltage higher than +50 V to prevent most secondary electrons to leave the electron gun. The restricted values of the focussing voltages off course limit the focussing possibilities of the gun, but this was not a problem during experiments.

Initially it was possible to do measurements of δ up to E_p=1000 eV. After several series of measurements it became clear that it was better to do the measurements up to higher energies. The reason for this is twofold.
The first reason is that for MgO, $E_{max} \approx 1000$ eV. Therefore it is difficult to say if the measured δ_{max} is correct. It may be possible that E_{max} lies at a higher energy resulting in a measured value of δ_{max} which is too low.
The second reason is that it turns out, that the problems with the surface barrier arising from an inhomogeneous surface charge distribution, occur when $V_A \approx 0$ V (Figure 3.6).
It was clear that when reliable measurements of δ_{max} were to be done, the set-up had to be modified.

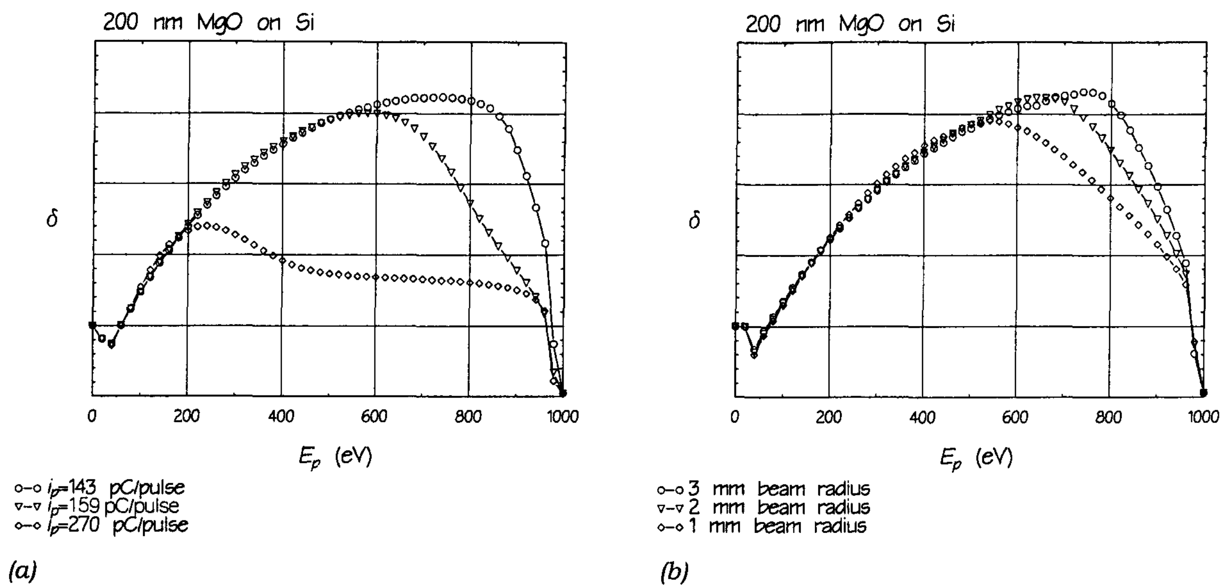

*-**Figure 3.6**- Due to an inhomogeneous surface charge distribution a major part of the secondary electrons is pulled back for energies above a certain E_p. For increasing j_p this energy decreases. In (a) the primary beam current is increased and in (b) the beam radius is varied. In (a) the beam radius is 4 mm and in (b), i_p=100 pC/pulse.*

To do measurements up to higher energies, another electron gun supply was needed. These supplies exist and are used for doing AES with the LEED optics. For setting V_A, now from -3.5 kV to 0 V, another HV supply was needed. This supply turned out to be very slow when it was switched from low to high output voltages. By simply loading the output of the supply with a high resistance a major decrease of the switching time was achieved, but still some delays had to be implemented within the computerprogram.
The resistance R_1, the capacitor C (Figure 3.1) and parts of the pulse generating circuit were replaced by super high voltage (SHV) components and to keep the set-up save, some coax sockets were replaced by SHV sockets.

The LEED set-up can also be used as a retarding field analyzer (RFA), with which Auger electron spectroscopy (AES) and measurements of the $N(E)$ distribution of secondary electrons can be done.
Doing AES with the RFA turned out to be very laborious. To do AES, a retarding voltage V_{ret} is applied to the middle two of the four grids. The electrons with an energy greater than $e \cdot | V_{ret} |$ will pass the grids and are collected by the screen. The integral of the $N(E)$ distribution from $e \cdot | V_{ret} |$ to E_{gun} is thus measured. To get $dN(E)/dE$, which in fact is the Auger signal, the integral has to be differentiated twice. This can be done by modulating the grids with a small voltage and using a lock-in amplifier. It can easily be shown that the Auger spectrum which is finally obtained is the *second* order term in the Taylor expansion around V_{ret} of the measured signal. This is the reason why the signal to noise ratio of this method is so low. To get a good signal the primary current has to be high, which gives charging problems. In addition the time constant of the lock-in has to be large, which causes a long sweep time which may influence the surface under consideration by electron stimulated desorption. Better spectra can be obtained with methods in which the signal is differentiated only once. An often used

example of an analyser which measures *N(E)* directly, is the cylindrical mirror analyser (CMA). During this work AES was done with an XPS/AES system which is connected with the LEED chamber. This system has a spherical energy analyser which also measures directly the *N(E)* distribution, which can be differentiated numerically.

§3.3 Sample Preparation

The films were grown in an OXI-MBE deposition apparatus. The XPS/AES as well as the LEED chamber were connected to this OXI-MBE deposition chamber, so the AES, LEED and SEE measurements could all be done *in situ*.
All experiments were done on in all 12 samples, made in six batches:

1. Three MgO films (thickness d=10 nm) with different crystal orientation (100), (110), (111),
2. Monocrystalline wedge-shaped layer (d=0-50 nm),
3. Polycrystalline wedge-shaped layer (d=0-50 nm),
4. Stepped MgO films on an n-Si and on p-Si substrate (d=5, 10, 20, 40 nm),
5. Three MgO films (100), (110), (111) (d=20 nm),
6. Mono- and polycrystalline wedge-shaped layers (d=0-50 nm).

For growing the *monocrystalline* MgO films of the first and fifth batch, MgO monocrystals were used as substrates. For the *monocrystalline* wedges, a $MgAl_2O_4$ monocrystalline substrate was used. There was no indication that the SEE properties of the MgO films were influenced by the choice of either of the substrates.
For the *polycrystalline* wedges, silicon substrates were used. The dimensions of all substrates were typically $l \times w \times h = 10 \times 10 \times 1$ mm^3.
Except for the MgO films of the fourth batch, which were grown directly on the silicon, first a 50 nm conducting Fe_3O_4 layer was grown upon the substrate. This layer was electrically connected to the sampleholder.
The wedge-shaped layers were grown by using a shutter positioned between the molecular beam and the target. This shutter was slowly pulled away during growth.
After the SEE measurements the thickness of the films was verified *ex situ* by RBS. XPS measurements in combination with sputtering were done to obtain a depth profile of the film composition.

The XPS measurements showed that the samples of the last three batches contained more oxygen (Table 3.1). This may be explained by the fact that these samples were grown several months later than the other samples. Therefore an unintentional change in the growing parameters may have occurred.

For the monocrystalline wedge shaped layer with the O/Mg=1.7, a LEED pattern was obtained, which was slightly worse than the LEED pattern of the monocrystalline wedge with O/Mg=1.2. It is unlikely however that with so many oxygen in the compound, the oxygen is restricted nore or less to local sites, in that way disturbing the LEED pattern. One would rather expect another crystal structure, for example

the spinel structure giving Mg_3O_4. This structure would cause extra LEED spots to appear. However, these were not observed. Furthermore, in the past it was attempted to grow MgO in the spinel structure, but this never succeeded.
Another reason for the differences in the oxygen magnesium ratio may be the presence of $Mg(OH)_2$ in the compound. This can be the result of a presence of water in the vacuum system during growth. Hydrogen cannot be observed directly by XPS. It can only be observed on further analysis of the Mg and O peaks in the spectrum. The magnesium and oxygen energy levels in $Mg(OH)_2$ are slighly different from the energylevels of these elements in the MgO compound, which can be observed in the XPS spectrum as a small energy shift of the magnesium and oxygen peaks.
The last possibility seems to be the most plausible for now. In the future more measurements must be done to determine the cause of the different oxygen magnesium ratios.

Table 3.1: O/Mg ratios of the different samples

Batch Number	O/Mg
1	1.2 ± 0.1
2	1.2 ± 0.1
3	1.2 ± 0.1
4	1.4 ± 0.1
5	1.5 ± 0.2
6 (poly)	1.5 ± 0.2
6 (mono)	1.7 ± 0.2

It is noted that the O/Mg ratios can only be compared relative to the other samples. The inaccuracy of the absolute values is larger than 0.2. Therefore the divergence from 1 is of no importance.

Chapter 4: Results

In this section the results of measurements of the SEE of several MgO films, characterized by the values for δ_{max}, E_{max} and E_I, are presented and discussed.
At room temperature MgO has a very high ohmic resistance ($R>10^{17}$ Ωcm^{-1}), therefore the SEE measurements are affected by charging effects which influence the SEE properties. The results of the measurements are presented as the measured *intrinsic* SEE, defined as the SEE not influenced by any effect of charging. Bearing in mind that the charging effects can be reduced but always will influence the measurements, one may suggest that it is of no practical use assuming the existence of such an intrinsic SEE. It may therefore be more correct to consider the charging effects as a part of the intrinsic SEE of insulators.
The reason why the results in this section are still presented as the SEE which approximates the intrinsic SEE, the SEE in case of an infinitesimal small i_p, are twofold.
The first motive is to follow the historically grown jargon.
The second reason is that intrinsic δ-curves are often used in numerical simulations of charging effects. In this kind of simulations an intrinsic δ-curve is input and the influence of charging effects is then calculated.
The measurements of the SEE are done with primary currents which are as low as possible ($i_p = \mathbf{O}(10^{-12}$ C/pulse) and with a defocussed beam (radius $R = 2.0 \pm 0.2$ mm).

§4.1 SEE at high primary energies ($E_p \gtrsim 100$ eV)

To study the influence of the sample thickness, two monocrystalline wedge-shaped MgO layers were grown. By measuring the SEE at different positions, information about the dependence of the SEE on the film thickness was obtained. The thickness of the layer varied from 0 to 50 nm.
The results of a mono- and a polycrystalline wedge-shaped layer are shown in figure 4.1.
The figure shows that δ_{max} increases with increasing film thickness. At small thicknesses there is a steep increase, but after a certain thickness δ_{max} becomes saturated. This saturation thickness is smaller in figure 4.1(b) than in figure 4.1(a). In the latter figure the saturated value is not even reached yet.
Another result is that the δ of polycrystalline MgO seems to be lower than that of monocrystalline MgO.

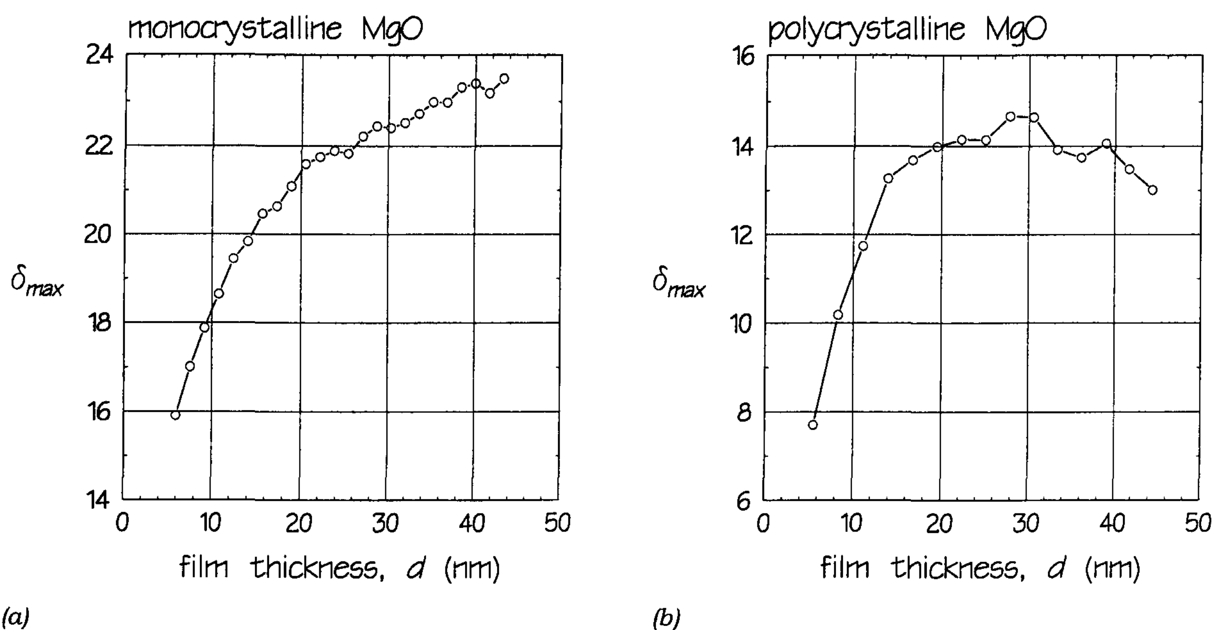

(a) *(b)*

Figure 4.1- *δ_{max} versus film thickness d for a mono- and a polycrystalline wedge-shaped layer. In (b) It seems that δ_{max} passes a maximum at $d \approx 30$ nm. This decrease is arteficial and caused by surface charging. This problem becomes more important in case of thicker and less crystalline samples. (E_{gun}=1000 eV, i_p = 5-7.5 pC/pulse and R=2.0 ±0.2 mm)*

The reason why δ_{max} increases and saturates is that in case of thin films, the measured δ is influenced by the Fe_3O_4 layer. A fraction of the primary electrons will create secondary electrons in the Fe_3O_4 layer, which has a lower δ than MgO. When the film thickness becomes greater than the escape depth of the secondary electrons, no influence of the Fe_3O_4 layer is measured anymore. All secondary electrons leaving the material are created within the MgO film and δ_{max} reaches a saturated value. For monocrystalline MgO this escape depth seems to be greater than 50 nm (Figure 4.1(a)). By extrapolating an escape depth of 75 nm can be estimated. For polycrystalline MgO, this escape depth seems to be 20 nm, but this estimation may be hampered by charging problems.

The lower value of δ_{max} of polycrystalline MgO films can be explained by the smaller escape depth of the secondary electrons in these films in comparison with monocrystalline films, due to the presence of more lattice defects. These defects will scatter the secondary electrons and thereby reducing the m.f.p. of the secondary electrons. A smaller escape depth will result in a lower δ, because less electrons are able to reach the surface and escape the film.
In this argument it is assumed that the penetration depth of the incoming electrons is less affected by the presence of lattice defects than the escape depth of the secondary electrons. This assumption is reasonable because the energy of the primary electrons ($E_{max} \approx 1000$ eV) is much higher than that of the secondary electrons ($E \approx 3$ eV).
The explanation above is supported by the experimental result that the saturation thickness for δ is greater for monocrystalline than for polycrystalline MgO. A smaller escape depth will cause a smaller saturation thickness because the contribution of the secondary electrons out of the Fe_3O_4 layer is cancelled at smaller thicknesses of the MgO film.

The wedges were grown in different batches. Although the samples were grown under the same conditions, some differences may have occurred. To check the intrinsic character of the earlier obtained results, the experiment with the two wedge-shaped layers was repeated later with two new samples made in one batch. Moreover measurements were done on these samples of $\delta(E_p)$ as a function of d, but now with primary energies up to 3.5 keV instead of 1 keV.
In figure 4.2 the results of the measurements are shown which are done under the same conditions as the measurements of the former samples.

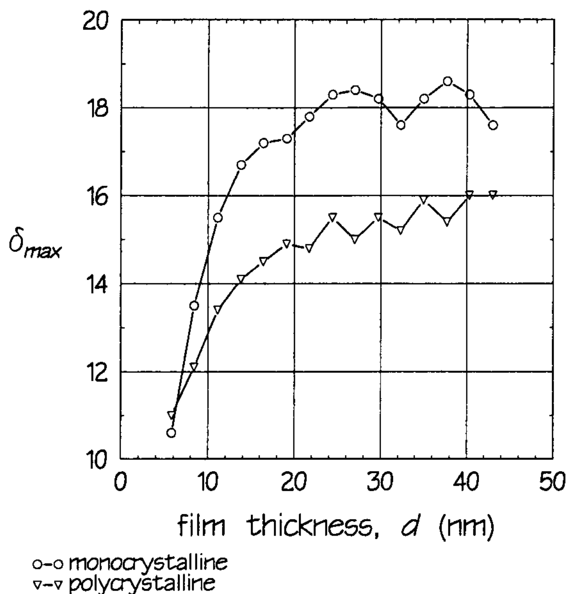

-Figure 4.2- *δ_{max} versus film thickness d for a mono- and a polycrystalline wedge-shaped layer. This figure should be compared with figure 4.1 (E_{gun}=1000 eV, i_p = 5-7.5 pC/pulse and R=2.0 ±0.2 mm).*

The shape of the curves looks quite the same as in the former experiments and the δ of polycrystalline MgO is again lower than of monocrystalline MgO.The saturated value of δ_{max} of polycrystalline MgO is about 15 for both wedges.
However comparing the two experiments, also some differences are observed. The saturation thickness of the first monocrystalline wedge is greater than that of the second (75 nm versus 30 nm for the latter wedge).
The LEED pattern of the first monocrystalline wedge was better than that of the second wedge. This indicates that the second wedge was less crystalline. It is assumed that this is caused by the high oxygen magnesium ratio which was observed for the latter three samples. This may explain the lower δ and the lower saturation thickness in terms of a smaller escape depth of secondary electrons, as well as the reduced difference in δ between the poly- and the monocrystalline wedge observed in the latter batch.
The results of the measurements of δ_{max} versus d on the two wedges done with the modified experimental set-up are shown in figure 4.3.

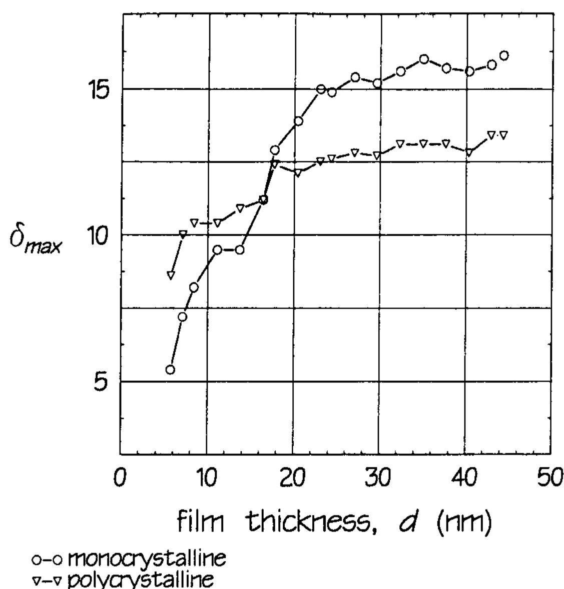

Figure 4.3- *δ_{max} versus film thickness d for a mono- and a polycrystalline wedge-shaped layers, both grown in the sixth batch. The measurements of $\delta(E_p)$ were done with the modified set-up with which measurements of δ up to 3.4 keV could be done (i_p = 5-7.5 pC/pulse and R=2.0 ±0.2 mm).*

Apart from a difference in δ , the curves of the polycrystalline samples in figure 4.2 and 4.3 look very much the same. The latter experiment was done several days later than the first experiment. Therefore the lower δ in figure 4.3 is probably due to a more contaminated surface, which is known to decrease δ.
The δ of the monocrystalline wedge has also decreased for the same reason, but besides that, the shape of the curve also looks different. The saturation thickness in the second experiment seems to be greater than in the first experiment (30 nm versus 40 nm) and the relative increase of δ with increasing d is higher.
The reason for this can be understood by looking at figure 4.4(a), in which E_{max} as a function of d is given. In figure 4.2 the measurements of δ were confined to $E_p <$ 1000 eV. For d≥20 nm, E_{max} exceeds 1000 eV, thus for d≥20 nm the measured δ_{max} is too low. For the experiments with the polycrystalline wedge this effect is smaller, because E_{max} does not exceed 1000 eV very much.
Note that for d≤15 nm δ_{max} is *smaller* for the monocrystalline wedge than for the polycrystalline wedge. Although it is less convincing in figure 4.2, it may be intrinsic. The reason for it is that, because of the greater escape depth of monocrystalline MgO, for thin films the underlying Fe_3O_4 layer, which has a lower δ than MgO, will give a greater contribution to δ than in case of a smaller escape depth. From figure 4.3, for polycrystalline MgO an escape depth of 20 nm is estimated.

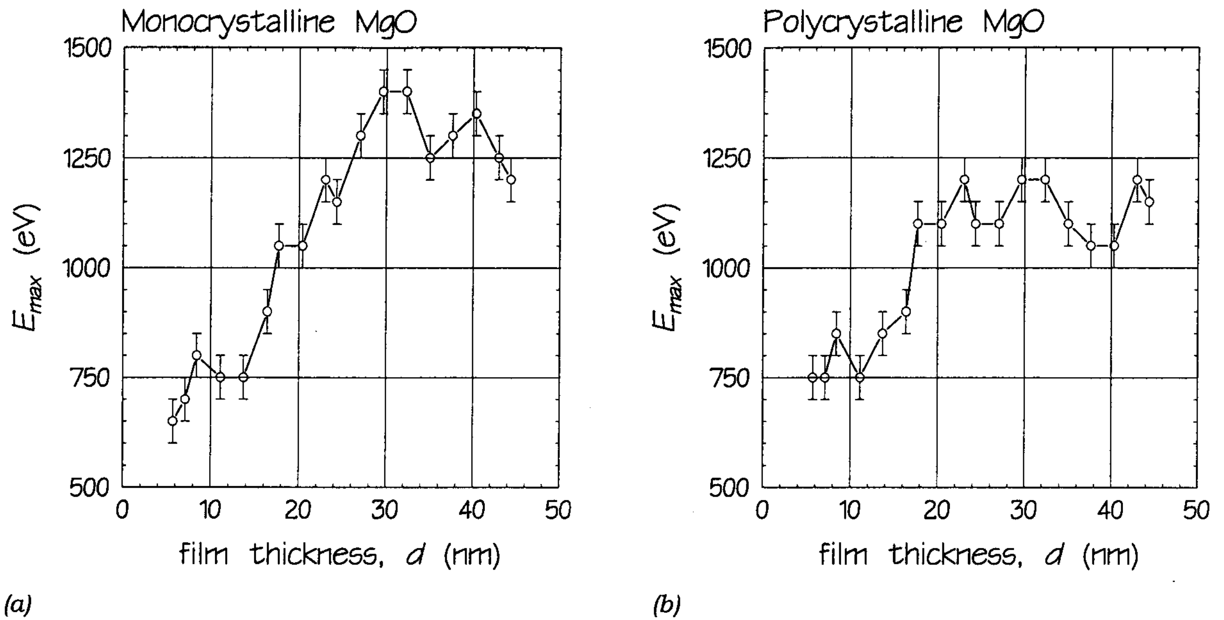

(a) *(b)*

Figure 4.4 *E_{max} versus film thickness d for a monocrystalline (a) and a polycrystalline (b) wedge-shaped layer, grown in the same batch.*

It is assumed that E_{max} is the primary energy at which the penetration depth of the primary electrons equals the escape depth of the secondary electrons. The higher value of E_{max} for the monocrystalline wedge at thicknesses beyond the saturation value is then again a verification of a greater escape depth in monocrystalline MgO.

Another explanation for the difference in δ between poly- and monocrystalline MgO may be a difference in δ for the different crystal faces. This may be caused by a different $E_g + \chi$. The surfaces of the monocrystalline wedges had the (100) crystal face. In case of a lower δ for the (110) and the (111) crystal faces, a lower δ for a polycrystalline film may be expected. To check this, three MgO films were grown in different lattice direction in one batch. The thickness of the films was 10 nm. The measured values of δ_{max} are given in table 4.2.
Notice that the δ_{max} of the MgO (100) film does very well reproduce the value for d=10 nm in figure 4.1(a).

The experiment was repeated later to check the reproducability of the measurements. However the film thickness was 20 nm instead of 10 nm, the δ of these samples turned out to be much lower (Table 4.2) than of the samples from the first batch. They do also not reproduce the value for d=20 nm in figure 4.2. From results of the XPS and RBS measurements no possible explanation could be found.
For now it is important that again only slight differences between the δ of samples with a different crystal face are observed.
The quality of the LEED patterns was best for the (100) sample and worst for the (111) sample. It is therefore not unlikely that the differences in δ_{max} of the different samples are caused by differences in the measure of crystallinity rather than by the difference in crystal orientation.

Table 4.2: δ_{max} of three MgO crystal faces.

Crystal Face	δ_{max} (1th batch, d=10 nm)	δ_{max} (5th batch, d=20 nm)
(100)	16.2	9.8
(110)	16.6	9.5
(111)	16.3	8.8

The results of the measurements of the MgO films of the fourth batch are shown in table 4.3.

Table 4.3: δ_{max} of the MgO films, grown on n- and p-Si.

Film Thickness	δ_{max} (n-Si substrate)	δ_{max} (p-Si substrate)
40 nm	11.3	11.6
20 nm	9.9	11.2
10 nm	9.9	10.1
5 nm	8.3	8.7

It seems that the δ of MgO on n-Si is slightly lower than that of MgO on p-Si. The measurements showed that the films on n-Si suffered more from surface charging than the films grown on p-Si, resulting in a more severe decay of the δ-curves. This is probably the reason for the differences in δ_{max}.
Another possibility can be a lower δ_{max} of n- than of p-Si. Because of the escape depth of 20 nm, part of the secondary electrons are generated in the substrate for $d \lesssim 20$ nm. It is unlikely however that this difference can be measured, because the difference in δ_{max} of n- and p-Si is probably much smaller than the differences in δ_{max} which are discussed here.

It is noted that the MgO films grown directly on Si, showed a more severe decay of the δ-curves than the films grown on Fe_3O_4. This may be caused by the fact that the conductivity of Si is lower than that of Fe_3O_4. Another aspect which plays a role is the presence of a thin insulating SiO_2 layer ($d \approx 2$ nm) between the MgO and the Si substrate. Although the substrate was annealed before growth, XPS measurements showed that the native oxide layer was not fully removed, probably caused by a bad thermal contact between the sampleholder and the Si substrates.
The fact that the MgO films which were grown directly on Si showed more charging problems, explains that for $d \gtrsim 10$ nm the measured SEE is lower than the values measured on the polycrystalline layers grown on Fe_3O_4.

§4.2 SEE at low primary energies ($E_p \lesssim E_1$)

The first cross-over energy, or E_1 point is the primary energy for which δ becomes 1 for the first time. Because for $E_p<E_1$ electrons are absorbed and for $E_p>E_1$ electrons are emitted, E_1 separates energy ranges in which fundamentally different phenomena occur. It is therefore important to know the correct value of E_1 .This energy is also an important parameter in describing the hop transport of electrons over the surface of an insulator.
Charging phenoma however always trouble the measurement of E_1. It is therefore a complex matter to separate the intrinsic behaviour of E_1 from charging effects. Moreover artefacts, due to the measuring method, may also hamper the measured value of E_1.
In this work many experiments were done in order to get a feeling about which physical quantities determine E_1 and on the other hand what has to be done to do a reliable measurement of E_1. An attempt was made to separate artefacts from parameters which determine the intrinsic value of E_1 .
This section contains the results of typical SEE measurements on several MgO films. Two artefacts which were thought of as being caused by artefacts were simulated.

§4.2.1 δ($E_p \lesssim E_1$) of MgO films

From measurements on the wedge-shaped layers no dependence of E_1 on the film thickness was found (Figure 4.5 and Table 4.4). This result is not very surprising because at these low energies the penetration depth is much lower than for $E_p \approx E_{max}$ in which region δ depends strongly on *d*. Because of this low penetration depth, the contribution of secondary electrons from the Fe_3O_4 substrate may disappear at thicknesses greater than 5 nm.
From these results it can also be concluded that a MgO film with a thickness of 5 nm, which is equivalent to 12 monolayers, behaves like bulk MgO as far as the SEE properties are concerned.

(a) (b)

-Figure 4.5- *Measurements of $\delta(E_p \lesssim E_1)$ as a function of the film thickness d for the wedge-shaped layers of the second and third batch. No strong dependence is observed.(i_p=7.0 pC/pulse, E_{gun}=200 eV, R=2.0 ± 0.2 mm)*

Table 4.4: E_1 of poly- and monocrystalline MgO as measured on the wedge-shaped layers of the sixth batch.

Film thickness	E_1 (monocrystalline)	E_1 (polycrystalline)
40.3 nm	15 ± 1 eV	14 ± 1 eV
19.1 nm	14 ± 1 eV	14 ± 1 eV

The crystallinity does not seem to influence the value of E_1 very much. For mono- and polycrystalline MgO, $E_1 \approx 15$ eV. Apparently the penetration depth of the primary electrons is in both samples lower than the escape depth of the secondary electrons in this primary energy range.

In table 4.5. the results for the MgO films with different crystal faces are given.

Table 4.5: E_1 of three MgO crystal faces.

Crystal Face	E_1 (1st batch)	E_1 (5th batch)
(100)	18 ± 1 eV	24 ± 1 eV
(110)	16 ± 1 eV	23 ± 1 eV
(111)	16 ± 1 eV	22 ± 1 eV

The results for the fifth batch shown in the third column of table 4.5 differ significantly from the values in the second column which are comparable to the

values in the second column and in the previous table. The reason for this is unknown. It cannot be caused by the high oxygen magnesium ratio which was found for these samples, because the wedge-shaped layers of the sixth batch and the films grown on silicon had the same O/Mg ratio but had a E_I comparable to the values in the second column (Table 4.4 and 4.6). Note that for the samples of the fifth batch also deviating values of δ_{max} were found (Table 4.2).

For MgO (100) E_I seems to be somewhat higher than for the other crystal faces. It is well known that most surface contaminants give an increase in E_I and a decrease of δ_{max}. But because the films differing in crystal orientation were grown in the same batch and the (100) surface is assumed to be least reactive, it seems that the deviant behaviour of the (100) surface cannot be explained by a more severe surface contamination. Moreover the δ_{max} of the MgO(100) films were somewhat higher or equal to the values of the other crystal faces.
An AES analysis of the surfaces after seven days in 10^{-9} Torr indeed showed more contaminated surfaces of the (110) and (111) crystal faces. All surfaces were contaminated particularly by carbon, for which $\delta_{max}\approx 1$ and $E_I \approx E_{max} \approx 300$ eV and fluorine. It is well known that C contamination decreases δ_{max} and increases E_I . On the other hand, MgF is a material which is assumed to have a higher δ_{max} and a lower E_I than MgO. Therefore a possible explanation for the deviant behaviour of MgO(100) is that it is less sensitive for F contamination than the other MgO crystal faces. The reason that δ_{max} is not found to be significantly higher for MgO(100), may be that for $E_p \approx E_{max}$ the secondary electrons are generated deeper in the film, which may diminish the influence of the surface absorbant.
Although this is a possible explanation more experiments have to be done to give a definite answer. For now it seems that with the current results, a larger spreading in the values of E_I has to be taken for granted.

Table 4.6: E_I of MgO films grown on n- and p-Si.

Film Thickness	E_I (MgO on n-Si)	E_I (MgO on p-Si)
40 nm	16.8 ± 0.8 eV	15.6 ± 0.8 eV
20 nm	19.0 ± 0.8 eV	15.2 ± 0.8 eV
10 nm	15.6 ± 0.8 eV	14.8 ± 0.8 eV
5 nm	15.0 ± 0.8 eV	14.8 ± 0.8 eV

In table 4.6 the results for the MgO films grown on n- and p-Si are given. Measurements of the surface potential (§4.3) and measurements of δ showed that MgO on n-Si charges more than MgO on p-Si. This may explain the higher values of E_I for d=20 and 40 nm of MgO on n-Si. During the measurement of E_I, the surface is charged negatively, because $\delta(E_p<E_I)<1$. This negative V_S decreases the effective E_p (§2.2) and therefore a higher E_I is measured. Thicker films suffer more from charging than thin films.
The increase of E_I with increasing d is not observed on the polycrystalline wedge-shaped layer. The reason for this is the presence of the conducting Fe_3O_4 layer in the latter sample. From different kinds of experiments it is observed that on MgO films grown directly on Si a surface potential is established more easily.

§4.2.2 Arteficial effects

In §3.1 it was pointed out how δ is measured. As explained earlier, E_p is determined by V_A. When a δ-curve is measured, a negative sample bias is first set to a value lower than $-E_{gun}/e$. In that case no electrons will arrive at the sample, i_n=0, and according to (3.1) a δ of 1 will be measured. When the sample bias increases beyond $-E_{gun}/e$, the first electrons will arrive at the sample and the δ-curve is measured. The measured curve should look like figure 4.6.

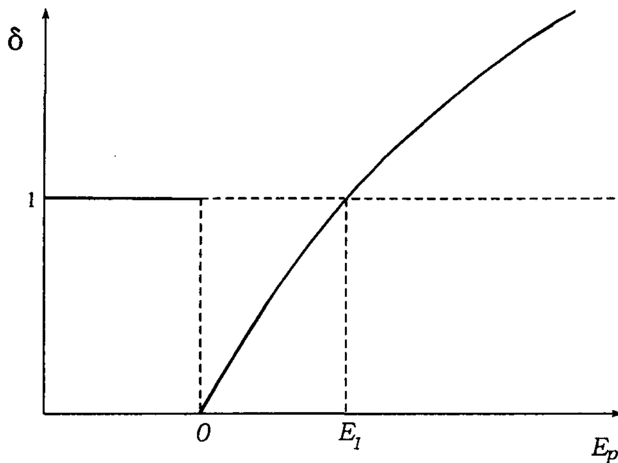

*-**Figure 4.6**- The secondary electron emission yield as a function of E_p. The figure shows how one would naively expect this curve to look like: with no artefacts.*

However, the measured curves look different. In figure 4.7 typical δ-curves are shown for a conductor and an insulator.

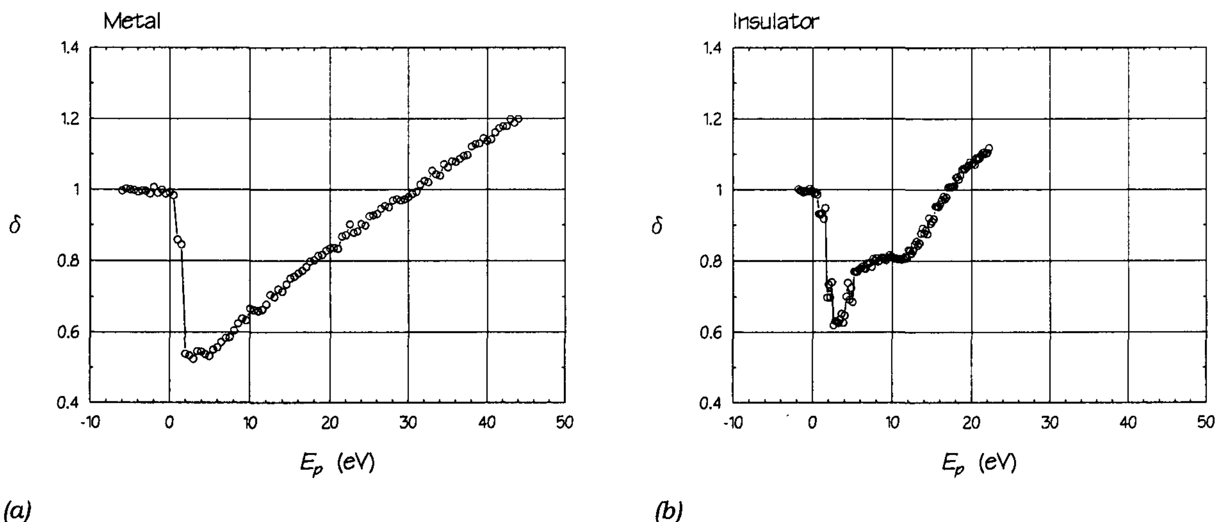

*-**Figure 4.7**- Typical low energy δ-curves as measured on a conductor (a) and an insulator (b). In (b) a knee is visible. The discrete steps which are visible on the δ-curves are artefacts. They represent the minimum step size of E_p, which is equal to 0.8 eV. The flatness of the steps is a measure of the noise of the measured values of δ.*

Because insulators are in general good electron emitters (§2.1.1), δ=1 will be reached at lower primary energies than in case of a metal. Therefore in general metals have a higher E_I than insulators.
In both figure 4.7(a) and figure 4.7(b) $\delta(E_p=0$ eV) does not reach 0. This could either be intrinsic or be the result of a defocussing effect of the electron beam. Defocussing results in an electron beam, which hits the surface with a perpendicular velocity, which is distributed over the surface. This will cause that only part of the electron beam reaches the surface at low primary energies.
Assume that electrons leave the electron gun with a top angle θ_0 (Figure 4.8).

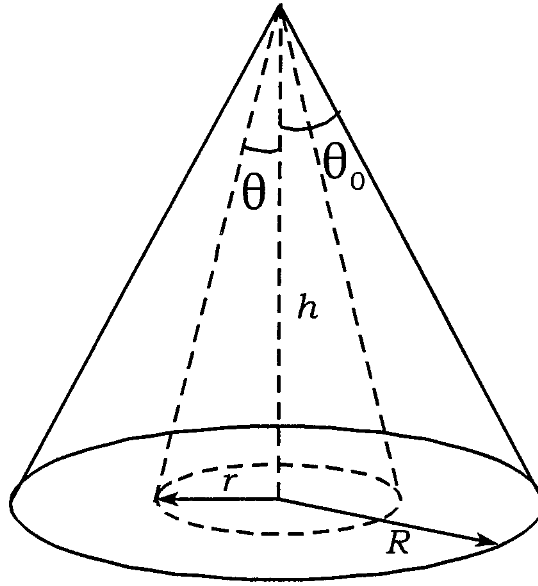

*-**Figure 4.8**- Schematic representation of the electron beam with radius R and top angle θ_0.*

An electron which leaves the gun with an energy E_{gun} , has a velocity perpendicular to the surface, which corresponds to

$$E_{\perp}(\theta_i) = E_{gun}\cos^2\theta\ , \tag{4.4}$$

in which θ is the angle of the initial velocity with the normal of the surface.
For a sample bias V_A only electrons will arrive at the sample for which

$$E_{\perp} \geq |V_A|. \tag{4.5}$$

From the two previous equations the angle θ_i within which all electrons will hit the sample, can be deduced. The result is given by

$$\theta_i = arccos\sqrt{\frac{|V_A|}{E_{gun}}}\ . \tag{4.6}$$

With

$$\tan\theta = \frac{r}{h}, \tag{4.7}$$

is found:

$$r_i = h\tan\left(\arccos\sqrt{\frac{|V_A|}{E_{gun}}}\right). \tag{4.8}$$

While measuring i_p, all current is measured, because a positive bias is used. When a measurement of the δ-curve is performed a negative bias is used and consequently only part of the primary current will arrive at the sample. The primary current which indeed reaches the surface is called i_p' and is given by

$$i_p' = i_p\left(\frac{\pi r_i^2}{\pi R^2}\right) = i_p\left(\frac{r_i}{R}\right)^2. \tag{4.9}$$

Finally, with (4.7) and (4.8) the following expression can be derived:

$$i_p' = i_p\frac{\tan^2\left(\arccos\sqrt{\frac{|V_A|}{E_{gun}}}\right)}{\tan^2\theta_0}. \tag{4.10}$$

For the measured value of the secondary electron emission yield, δ ', is then found

$$\begin{aligned}\delta'(E_p) &= 1-\frac{i_n'}{i_p} = 1-\frac{i_p'-i_s'}{i_p} = 1-\frac{i_p'}{i_p}[1-\delta(E_p)] = \\ &= 1-\frac{\tan^2\left(\arccos\sqrt{\frac{|V_A|}{E_{gun}}}\right)}{\tan^2\theta_0}[1-\delta(E_p)].\end{aligned} \tag{4.11}$$

From this equation an influence can be expected of E_{gun} and θ_0 on the δ-curve. This is also shown in figure 4.9 and 4.10.

It has been shown in these figures, that if an effect should exist due to defocussing, a clear dependence on the gun energy and on the defocussing should exist for both metals and insulators. All experiments were done with $R \lesssim 2.0$ mm. With $h \approx 35$ mm, $\theta_0 \lesssim 3.3°$ is found. According to figure 4.9, for $\theta_0 = 3.3°$, a strong dependence on E_{gun} can be expected.

Measurements on metals seemed to show some of the predicted effects. For the first 5 eV, δ seemed to increase with increasing E_{gun} and θ_0, but far too little to explain the fact that $\delta \neq 0$ for $E_{gun} = e \mid V_A \mid$. Moreover, the effect is much smaller than is expected from the calculations. The reason for this is probably that the experiments were done with a smaller θ_0, than the estimated value based on the beam radius. The value of θ_0, calculated with (4.7), is in fact an upper limit. In reality, the electron beam will be less diverging and therefore the value of θ_0 will be smaller.

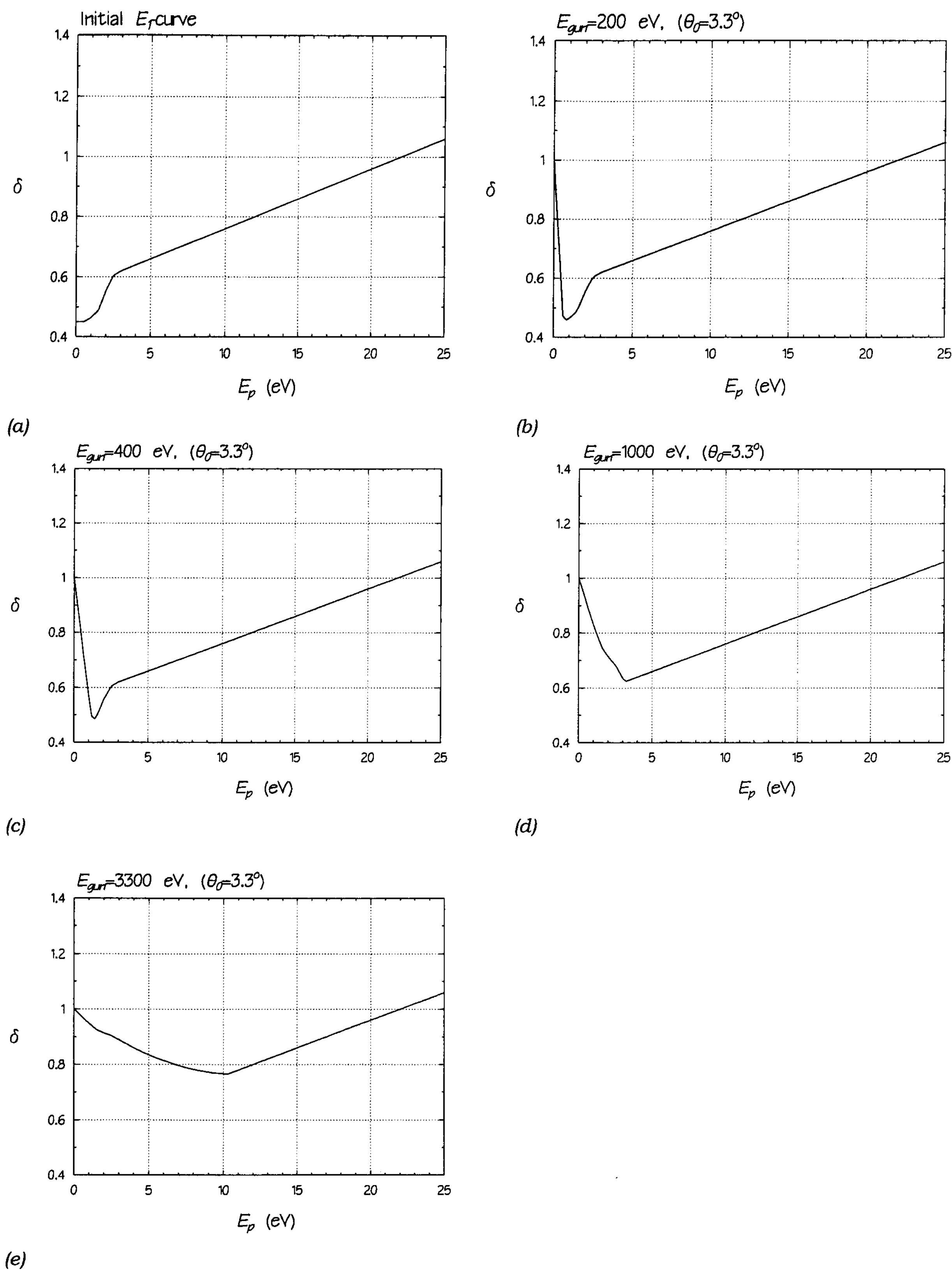

Figure 4.9- *Simulation of the influence of E_{gun} on the δ-curve for θ_0=3.3°*

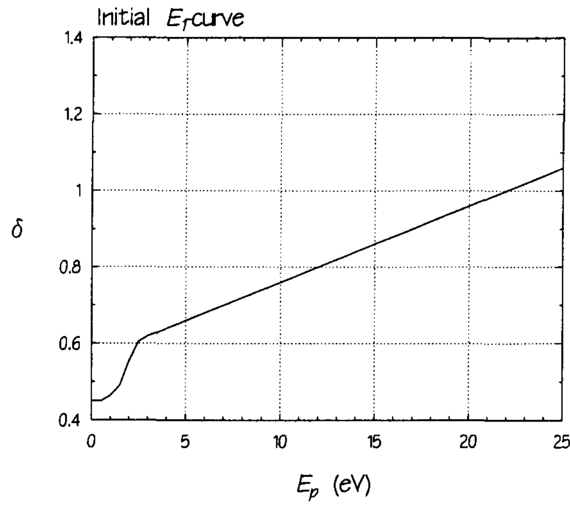

(a)

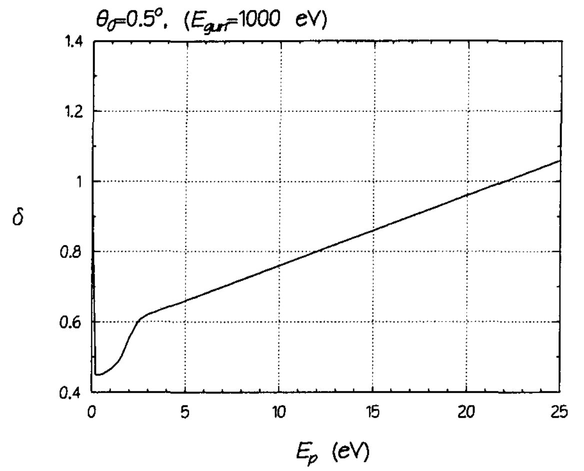

(b)

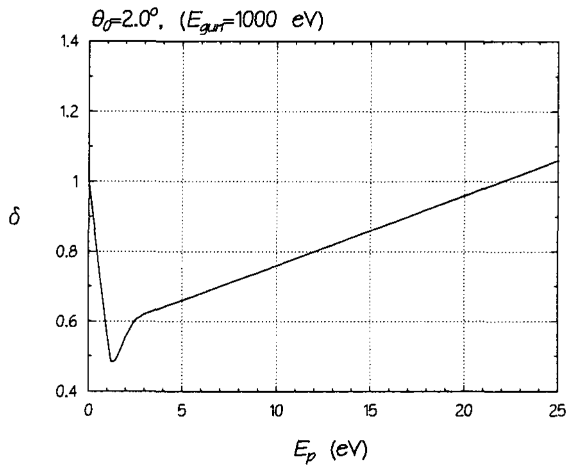

(c)

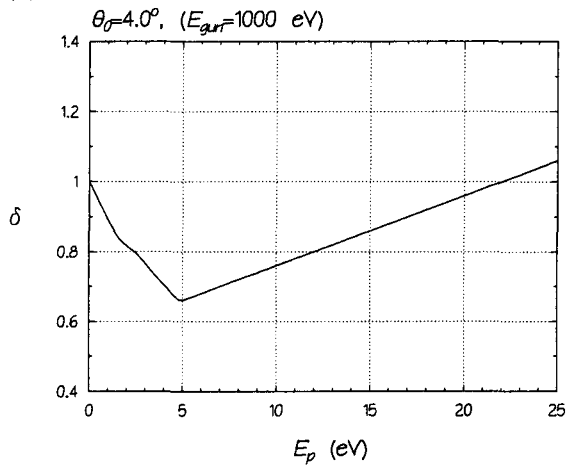

(d)

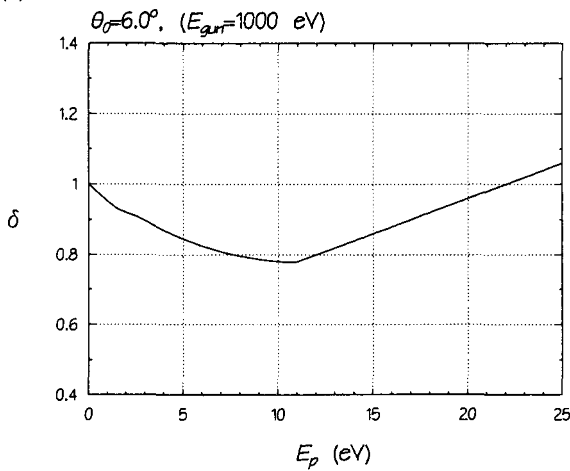

(e)

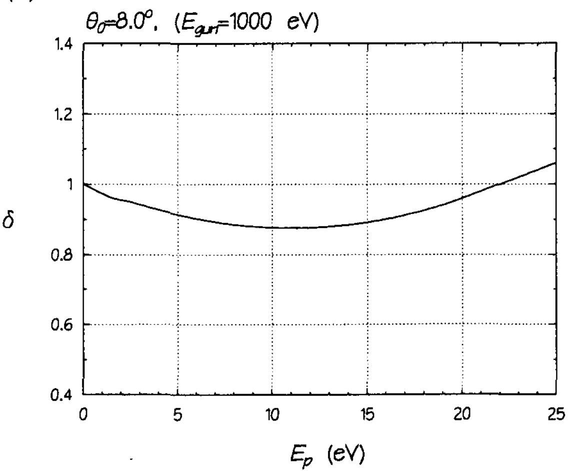

(f)

-Figure 4.10- *Simulation of the influence of θ_0 on the δ-curve for E_{gun}=1000 eV.*

In figure 4.11 and 4.12 results are shown of measurements on a 40 nm MgO film grown on p-Si and are typical for insulating samples. Measurements on other MgO films and on SiO_2 gave similar results. In these figures the influence of respectively E_{gun} and R is shown. Now a clear dependence of δ on E_{gun} and R is visible. The SEE yield increases for increasing E_{gun} and for a more defocussed electron beam also a shoulder appears at the beginning of the δ-curve. These effects are only seen on insulators and can therefore not be explained by the defocussing effect mentioned before.

The dependence of δ on E_{gun} and R may be the result of a potential distribution on the surface of the sample. This potential distribution, which is generally negative, will just as the defocussing effect, result in a decrease of the effective primary current.
Assume that we have a circular symmetric surface potential: $V_S(\mathbf{r})=V_S(r)$. The contribution of the primary electrons with $r'<r<r'+dr'$ to the secondary current i_s' is

$$di_s' = i_p \frac{dO}{O} \delta(E_{gun} + e \cdot V_A + e \cdot V_S(r)) . \tag{4.12}$$

With $dO/O=2rdr/R^2$ is found

$$i_s' = i_p \frac{2}{R^2} \int_0^R \delta(E_{gun} + e \cdot V_A + e \cdot V_S(r)) r dr . \tag{4.13}$$

Furthermore

$$\begin{aligned} i_p' &= \int_0^R i_p \frac{dO}{O} \Theta(E_{gun} + e \cdot V_A + e \cdot V_S(r)) r dr = \\ &= \frac{2 i_p}{R^2} \int_0^R \Theta(E_{gun} + e \cdot V_A + e \cdot V_S(r)) r dr, \end{aligned} \tag{4.14}$$

where $\Theta(x)=0$ for $x<0$, in which case no electrons can reach the surface, and $\Theta(x)=1$ for $x>0$.
With $\delta' = 1-(i_p'-i_s')/i_p$ this finally yields

$$\delta' = 1 - \frac{2}{R^2} \int_0^R [\Theta(E_{gun} + e \cdot V_A + e \cdot V_S(r)) - \delta(E_{gun} + e \cdot V_A + e \cdot V_S(r))] r dr . \tag{4.15}$$

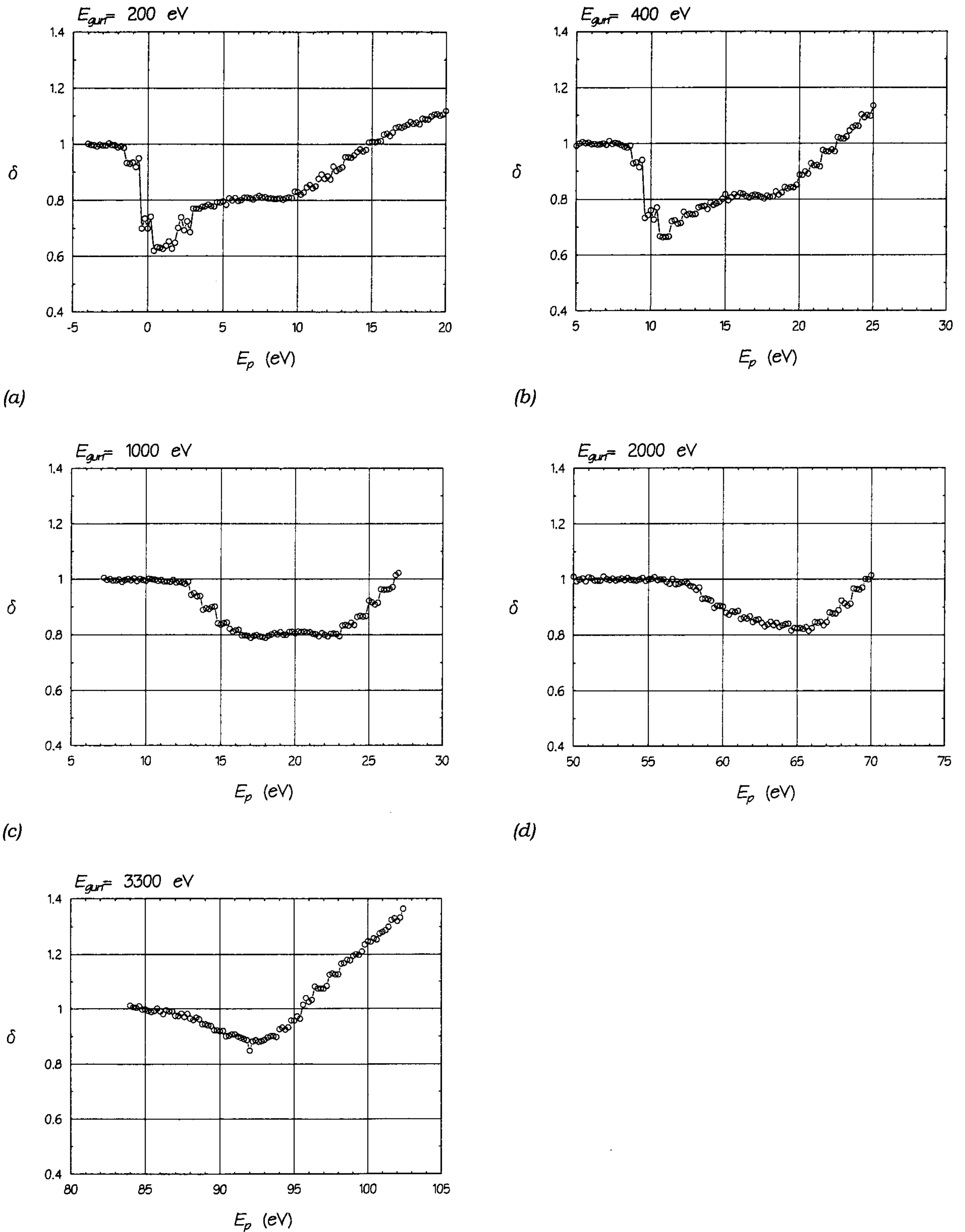

-**Figure 4.11**- *δ-curves at low energies for different values of E_{gun}. The curves were measured on a 40 nm MgO film on a p-Si substrate. For all measurements $i_p \approx 10.5$ pC/pulse, $R \approx 0.15 \pm 0.05$ mm, $\theta \approx 0.21°$. The δ-curve does not start at E_p=0 eV because of the non-linearity of the HV-supply setting V_A (2-3%).*

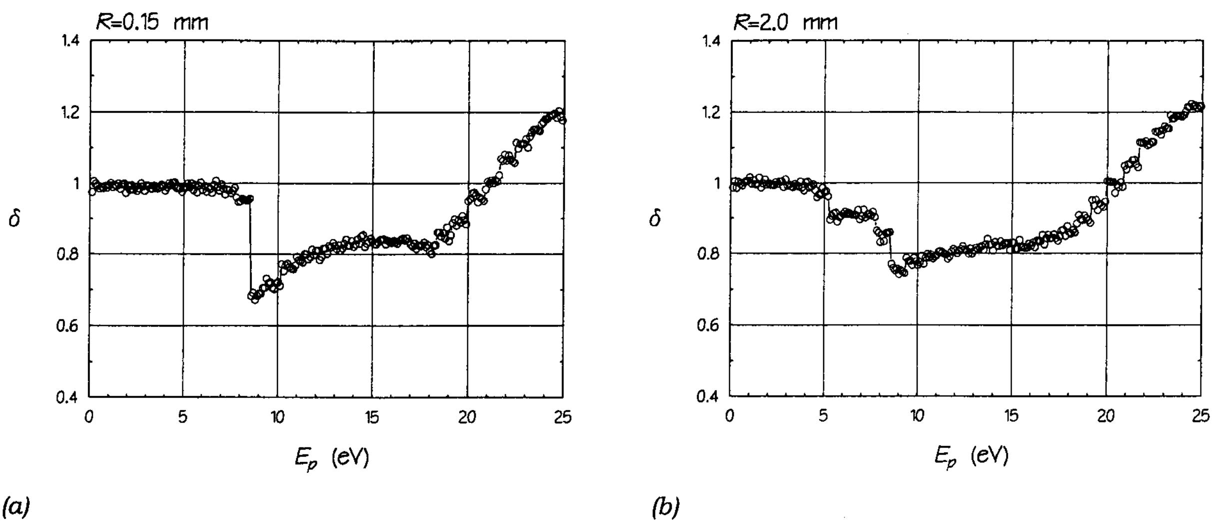

*-**Figure 4.12**- δ-curves at low energies for two different values of R. The curves were measured on a the polycrystalline wedge shaped layer of the sixth batch (d=27 nm, $i_p \approx 8.0$ pC/pulse and E_{gun}=200 eV). In (b) the dip at 8.5 eV is less deep, a shoulder appears at the beginning of the curve and the dip at 18 eV has dissappeared*

With (4.15) the influence of a certain V_S *(r)* was calculated. The best results were obtained with a V_S *(r)* as shown in figure 4.13.

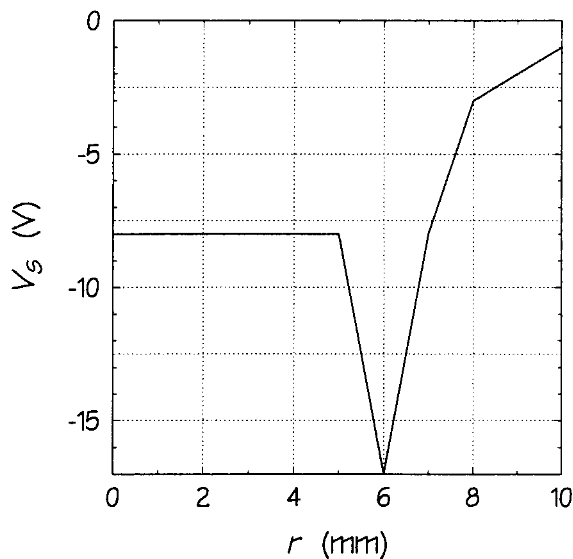

*-**Figure 4.13**- Typical shape of Vs (r) as used in the calculations.*

In the past such shapes of $V_S(r)$ were obtained by Monte-Carlo simulations of electron trajectories done by Ying [16] and Hendriks [15] (see also figure 3.3).
The intrinsic δ-curve from which the calculations were started, was assumed to have the shape characteristic for metals, without a knee (Figure 4.7). This was done, because experiments indicate that this knee is not intrinsic, but a charging

effect. A first argument is that on a conductor such a knee is never observed. Measurements on MgO (100), (110) and (111) showed subtle differences (Figure 4.14). The knee in the δ-curve of MgO(110) is significantly less than in the MgO(100) and (111) films. Moreover, measurements of the surface potential indicated that the MgO (110) film charged most. Additionally, measurements on the wedge-shaped layers showed a bigger knee for the thicker films.

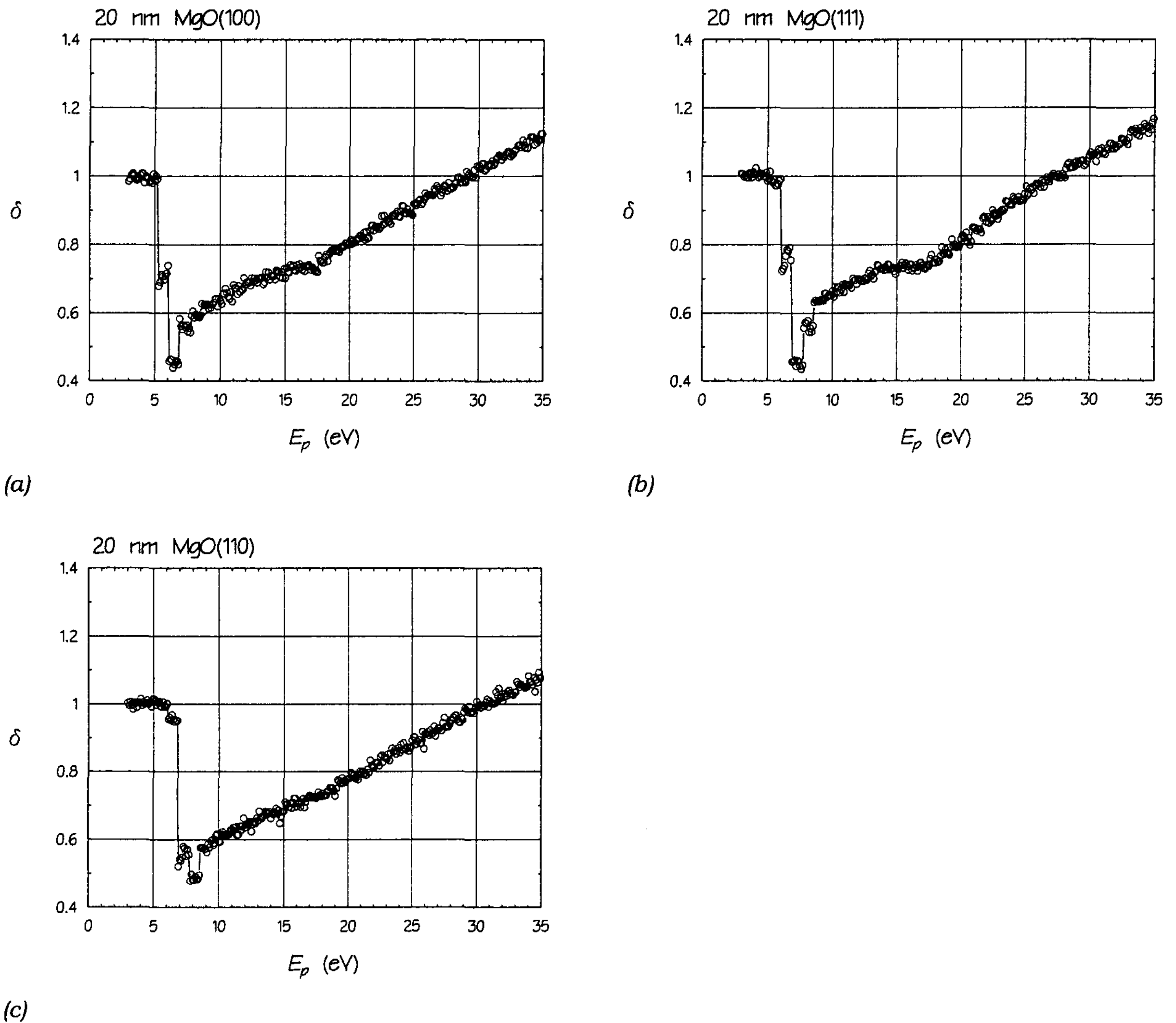

*-**Figure 4.14**- Measured δ-curves at low energies of MgO films with different crystal faces.*

The results of the calculations are shown in figure 4.15. Note the striking resemblance between the figures 4.15(c) and 4.12(a) and the figures 4.15(f) and 4.12(b).

For r<5 mm $V_S(r)$ is constant and the δ-curve is shifted towards higher energies is equal to $e \cdot |V_S|$. The curve shape remains unaltered.

For 5<r<7 mm a knee is formed and the dip becomes less deep. It is apparently caused by the negative peak in $V_S(r)$ for these values of r. It can be understood as follows. The primary electrons which see the potential $V_S(5<r<7$ mm$)$ are retarded

more than the primary electrons impinging at r<5 mm and for low values of E_p these electrons cannot even reach the surface. This causes a decrease of the effective primary current. Reminding $\delta' = 1-(i_n'/i_p)$, this results in an increase of the measured value of δ.
For higher values of E_p when in spite of the retarding surface potential all primary electrons can reach the surface, δ' will be damped. Due to the lowered E_p for the primary electrons impinging with $5<r<7$ mm these electrons will generate less secondary electrons than the primary electrons for which $r<5$ mm and therefore the total amount of secondary electrons decreases.

For $r>7$ mm the shoulder becomes visible, which becomes deeper for increasing r. The formation of the shoulder is caused by the fact that the electrons at the edge of the beam are less retarded than the electrons in the inner area of the e-beam. These outer electrons will reach the surface for lower values of $|V_A|$ which occurs as a shoulder in the δ-curve. The latter result was already obtained by Schmitz [17]. Note that for $r>5$ mm the dip becomes less deep due to an decrease of the effective i_p.

From the foregoing it can be concluded that the different shapes of the δ-curve at low energies, found for insulators and metals, can fully be explained by the presence of a surface potential distribution in case of an insulating sample. The shape of the surface potential distribution, which gives the best resemblance between the measured and the simulated δ-curves, looks very similar to that established during the measurement of the primary current. Therefore it is possible that the different shapes of the measured δ-curves, obtained with different values of E_{gun} and R (Figure 4.11 and 4.12), are caused by a different surface potential distribution, established during the measurement of i_p. Preliminary experiments have confirmed this assumption. The primary current was measured with certain fixed values of E_{gun} and R. With this calibration, δ-curves were measured for different values of E_{gun}. With this method, every experiment is started with the same initial surface potential distribution. It turned out that the measured δ-curves were independent of E_{gun}.

In figure 4.6 the δ-curve starts at 0 eV. In §2.1.1 it was mentioned that secondary electrons can be generated for $E_p \geq E_g - \chi$, or $E_p \geq \phi$ in case of a metal. One would therefore expect the δ-curve to start at $E_p = E_g - \chi$ ($E_p = \phi$) in first instance. Remind however that with the used measuring method, i_s is not measured directly, but that i_n is measured. When the primary energy is too small to generate secondary electrons, still $i_n \neq 0$ will be measured, because part of the primary electrons is absorbed in the material. Therefore the measured δ-curve will start at E_p=0 eV.
The minimum step size of E_p is 0.8 eV. Therefore the reason why $\delta(E_p=0$ eV) seems not to start at 0, can be explained by the assumption that the absorbed part of the primary current rises to a nonzero value within 0.8 eV, which makes the rise undetectable. To check this, the resolution of the set-up has to be increased, by decreasing the minimum step size.

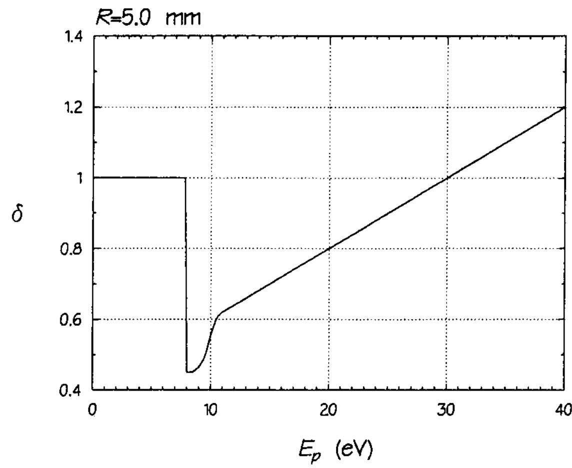

(a)

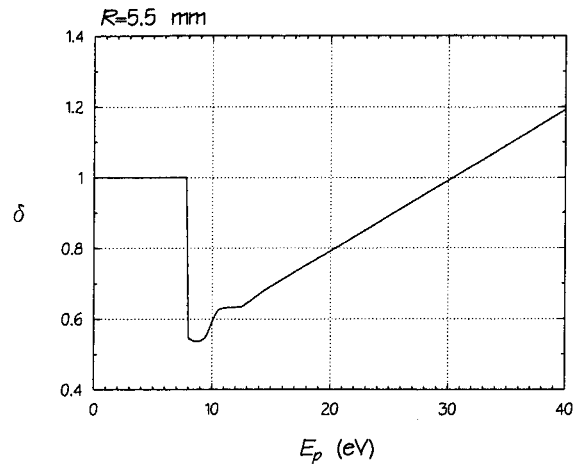

(b)

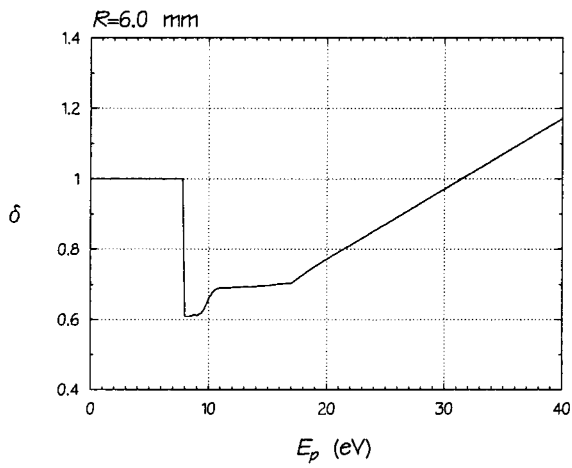

(c)

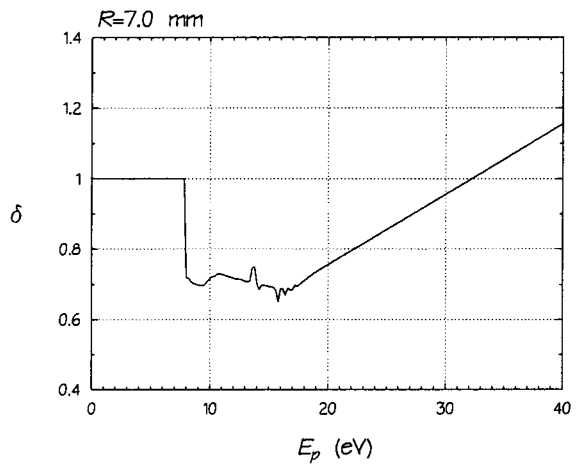

(d)

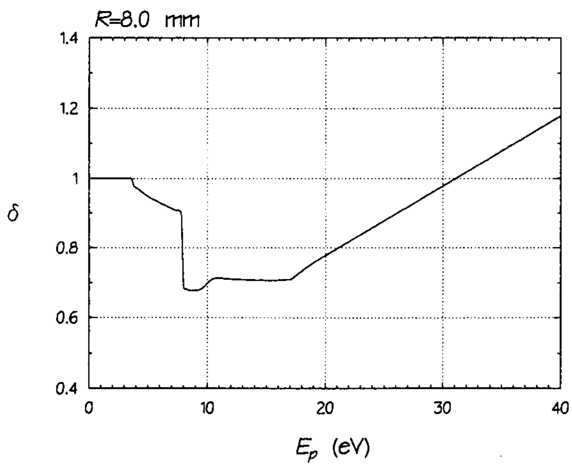

(e)

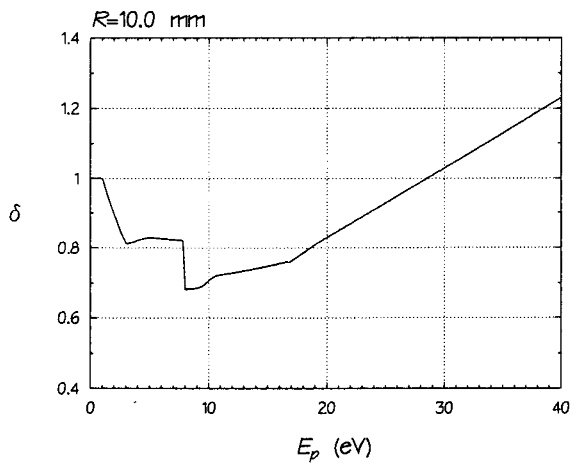

(f)

*-**Figure 4.15**- Simulation of the influence of the beam radius R on the δ-curve, in the presence of a surface potential distribution* $V_S(r)$.

§4.3 Surface Potential Measurements

In the preceding sections it was found that the surface potential distribution influences the measured δ, both for low primary energies and high energies. In this section the results are presented of measurements of the surface potential.

When the surface potential V_S of a sample is greater than zero, the primary electrons will be accelerated towards the sample. Their actual kinetic energy at the surface will therefore be higher than in case of V_S =0 V. The onset of the measured δ-curve will therefore shift to lower energies which follows directly from the measuring method of δ described in §3.1. In the same way, for V_S <0 V the onset will shift to higher energies, because the primary electrons are retarded now.
In §4.2 it was found that when the shoulder is absent, the onset of the δ-curve is determined by the first part of V_S which is constant (Figure 4.13), the so-called *core potential.* Information about V_S in the outer area, r>5 mm in figure 4.13, can be obtained by an interpretation of the shape of the δ-curve.

For a correct measurement of V_S, first a measurement on the conducting sampleholder was done. When measuring a δ-curve, it will in general not start at 0 eV. The reason for this is that the HV supply is not perfectly linear, but has a deviation of some 2 or 3%. For an E_{gun} of 1000 eV, this means that the onset for the δ-curve may be shifted by 20 to 30 eV, due to the spreading in V_A (see (3.1)). For the measured value of V_S then holds

$$V_S = -(V_{onset}^{MgO} - V_{onset}^{SH}) , \tag{4.16}$$

in which 'SH' stands for 'sampleholder'. To induce a certain surface potential, the surface under consideration was bombarded with electrons for one minute with a pulse repetition time of 10 μs and a pulse duration of 5 μs. It was observed that when the MgO films under consideration were bombarded with electrons while V_A>0 V, a certain saturated surface potential was established. Another saturated value of the surface potential was established when V_A <0 V. It is assumed that these saturated states are dynamical equilibrium states, in which the removal of charge at the surface, due to certain conduction mechanisms, is equal to the pile up of charge described in §2.2.
Although the settling time of the equilibrium state was found to be shorter than 30 seconds pulsing time for all studied samples, a pulsing time of 60 seconds was used to make sure the steady state had been established.
By studying the established core potential as a function of i_p for different samples, information about the charging and conduction mechanisms in MgO films may be obtained.
The experiments discussed below were done in the following way. At first a measurement of the set i_p was done following the procedure as described in §3.1. Then V_A was set to +200 V and for one minute the surface was pulsed with the set i_p after which the onset of the δ-curve was measured. While doing this, the

computerprogram was run in the *fixed calibration mode*, because a measurement of i_p may change the induced surface potential. After that V_A was set to -200 V and the surface was pulsed again with the set i_p for one minute. Subsequently the onset of the δ-curve was measured again. The primary current was then set to a higher value and the procedure was repeated.
It is noted that relaxation effects may trouble the results of the measurements. To get an idea about the importance of such effects a measurement of the 1/e relaxation time of a 40 nm MgO film upon a p-Si substrate was done. This relaxation time could be estimated to be longer than 7 hours, which is too long to change V_S significantly between the creation and measurement of the core potential.

In figure 4.16 the result of such a measurement is shown. The experiment was done on the polycrystalline wedge of the third batch.

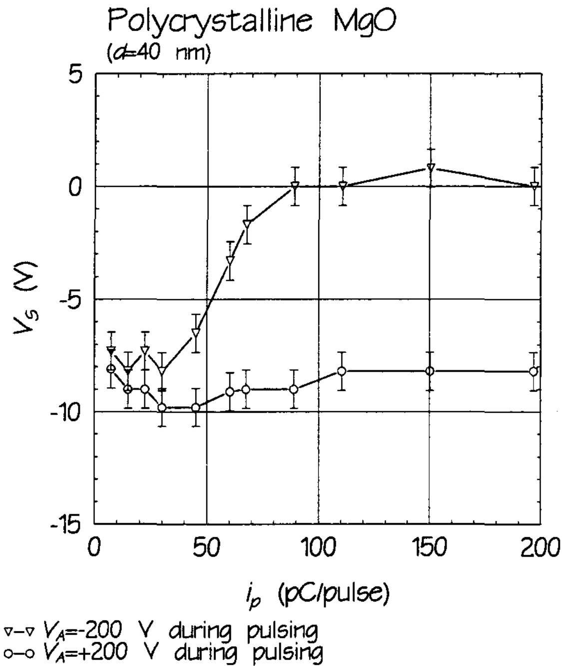

-Figure 4.16- *The induced surface potential as a function of i_p for a polycrystalline surface. This experiment was done with a defocussed beam (R=2.0 ± 0.2 mm) and E_{gun}=1000 eV.*

The figure shows a negative surface potential at low primary currents. There is only a small difference between the two pulsing modes. The surface potential starts to rise when $i_p \geq 40$ pC/pulse and V_A =-200 V during pulsing (d.p.), while the potential induced with V_A =+200 V d.p. hardly changes. For $i_p \geq 90$ pC/pulse both surface potentials seem to reach a saturated value. For V_A =-200, +200 V d.p. these values are 0 V and -8.2 V respectively.
To check that the measured negative potential was not already on the surface before the experiment was started, it was tried to reproduce the surface potentials at low i_p after the last measurement, which was done at high i_p. It turned out that the potential measured at low i_p, starting from a surface potential induced by the

high i_p, were indeed reproducible. It can thus be assumed that the surface potentials measured at low i_p are induced by these currents and that they are independent of the initial values before pulsing. Moreover from this reproducability it can be assumed that the sudden rise of the surface potential at high values of i_p is not caused by a breakdown in the MgO.

For V_A=+200 V d.p., the same mechanism occurs as during the measurement of i_p (figure 3.3). It is therefore not surprising that a negative core potential is found. For V_A=-200 V d.p., one would expect a positive surface potential, because during pulsing, E_p=1000-200 eV=800 eV>E_I . It was shown in §2.2 however, that this reasoning is only valid when the surface is homogeneously charged. This situation is approximated when the spot diameter is very large. Ying [16] showed, that for small spot diameters an inhomogeneous surface potential distribution is induced. Monte Carlo simulations were done and they showed that at the *beginning* of the irradiation the irradiated core indeed charges positively. This core is surrounded by a negatively charged ring, just as in figure 3.3. Such a ring of negative charge has the effect of introducing a potential barrier above the core, that prevents a part of the secondary electrons leaving the sample. Electrons that land within the core neutralize its positive charge, while electrons that land beyond the core, charge the surrounding insulator negative. The calculations of Ying show that at further charging, the electrons landing outside the core tend to land more inwards, resulting in a decreasing potential of the negative charged ring. This increases the surface barrier at the core and after the core potential initially charged positively, it drifts downwards to a negative potential. The shape of the potential distribution looks very similar to the one obtained by Hendriks (figure 3.3).
It seems that the charging mechanisms of the surface are qualitatively the same for negative and positive values of V_A. It is likely however that the sign of V_A will influence the surface potential to a certain extend. For example with V_A=+200 V d.p., the whole sample will charge negatively, because of hopping of electrons (x>0.004 mm in figure 3.3). In case of V_A=-200 V d.p., this hopping will not occur, because of the absence of an electrical field acting as a transport field. Therefore in case of V_A=-200 V d.p., the charged area will be smaller. It is also not unlikely that the sign of V_A will influence the depth and the width of the potential dips.
It is observed that at a certain i_p, for V_A=-200 V d.p. the surface potential starts to rise. As said before, the induced surface potential is a dynamical equilibrium and it is possible that at these high currents, the mechanism as described above does not work anymore. Apparently the subtle charging mechanism caused by a local surface barrier at the core is disturbed and the charging will act more as is expected from the sign of δ.

In figure 4.17 and 4.18 the results are presented for the wedge-shaped layers of the 6th batch The experiments were done with a focussed beam (R=0.15±0.05 mm).

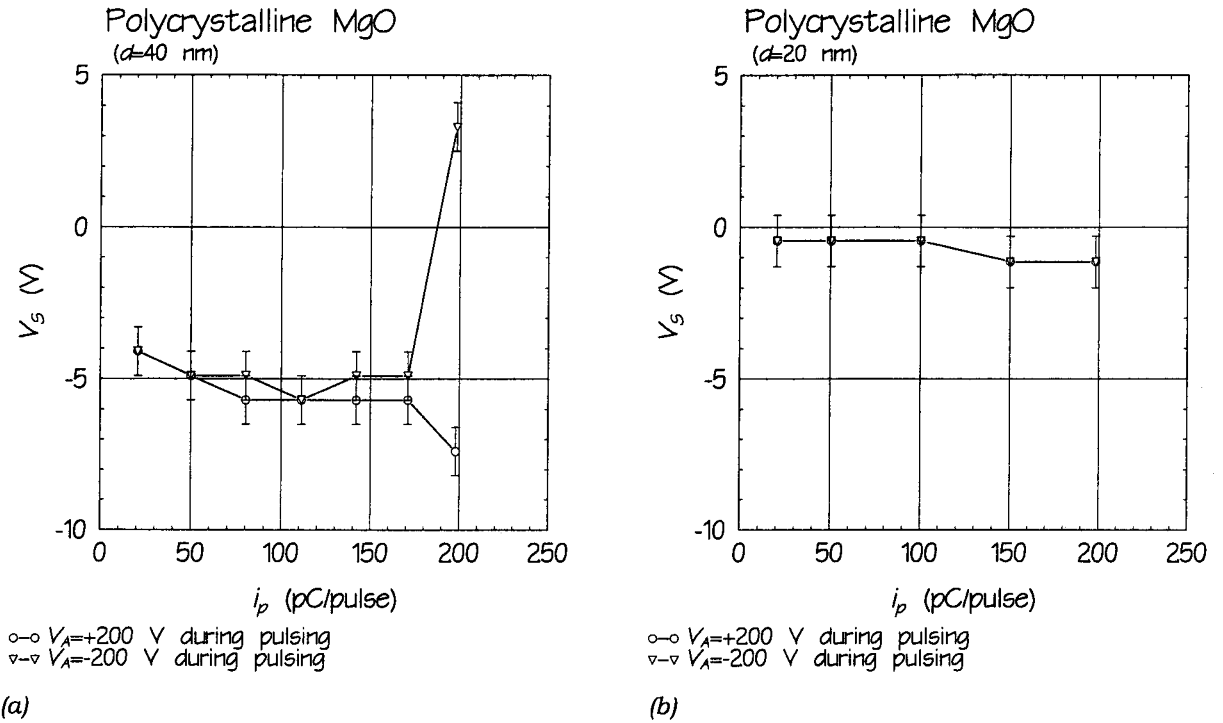

-Figure 4.17- *The induced surface potential as a function of i_p for the polycrystalline wedge of the 6th batch. In (a) the film thickness d is 40 ± 1 nm and in (b) d=20 ± 1 nm. (E_{gun}=1000 eV and R= 0.15 ± 0.05 mm)*

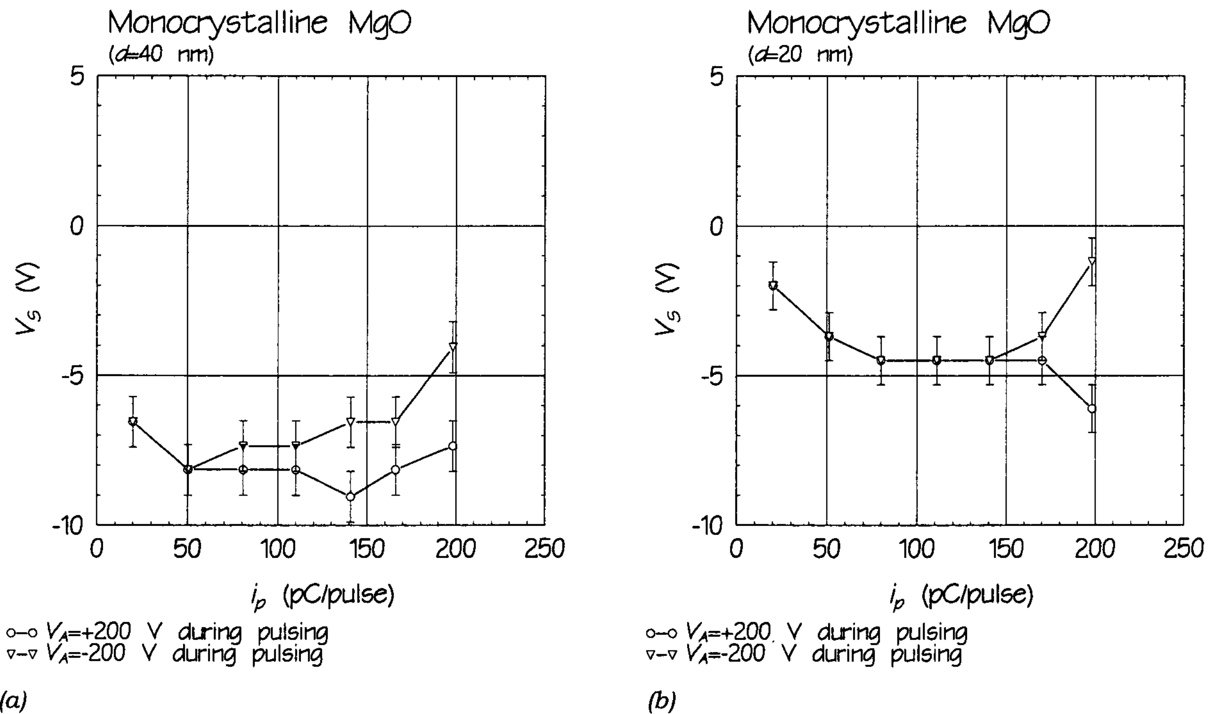

-Figure 4.18- *The induced surface potential as a function of i_p for the monocrystalline wedge of the 6th batch. In (a) d=40 ± 1 nm and in (b) d=20 ± 1 nm. (E_{gun}=1000 eV and R= 0.15 ± 0.05 mm)*

Again it is observed that for low values of i_p the induced potential is negative for both pulsing modes and that there is an onset current for which the induced V_S starts to differ for the two modes.
There is no saturation visible of the two induced surface potentials, but the i_p at which this saturation occurs may be higher than 200 pC/pulse.
The figures also show that the surface potential is higher for the polycrystalline sample than for the monocrystalline sample. It is not possible to relate the measure of decay of the δ-curve, which is higher in case of polycrystalline MgO, to the measured value of V_S for these samples. The reason for this is that only the core potential is measured, which gives no direct information about the surface potential barrier.
Both samples are less charged for d=20 nm than for d=40 nm, which can be understood by the decreasing resistance of the film with decreasing thickness, giving another equilibrium state.

Note that figure 4.16 differs from figure 4.17 in the threshold value of i_p beyond which V_S starts to rise. Moreover, the potential is more negative for i_p lower than the threshold value. The experimental conditions during the measurement of V_S were different for the wedge of the third batch. The beam radius in the first measurement was lower, which will certainly influence the induced potential distribution. Moreover, at the moment the measurement was done, the sample had spent 13 days in 10^{-9} Torr. For the other measurements this was 4 days. Thus the first wedge was more contaminated than the latter ones.
Therefore a quantitative comparison of the measurements does not make much sense. The qualitative behaviour however seems to be the same for both samples and in Figure 4.16 the saturation of V_S for high values of i_p is clearly visible.

Note that the negative potential for low i_p is also a saturation value, because in the limit $i_p \downarrow 0$, the surface potential must go to 0 V. In figure 4.17 and 4.18 the saturation is observed and occurs for $i_p \approx 75$ pC/pulse. It is possible that for all the other samples, on which this is not observed, this saturation value of the surface potential is reached for values of i_p lower than the smallest i_p with which was measured.

Measurements on the second batch of samples with a different crystal face also showed a comparable behaviour (Figure 4.19).

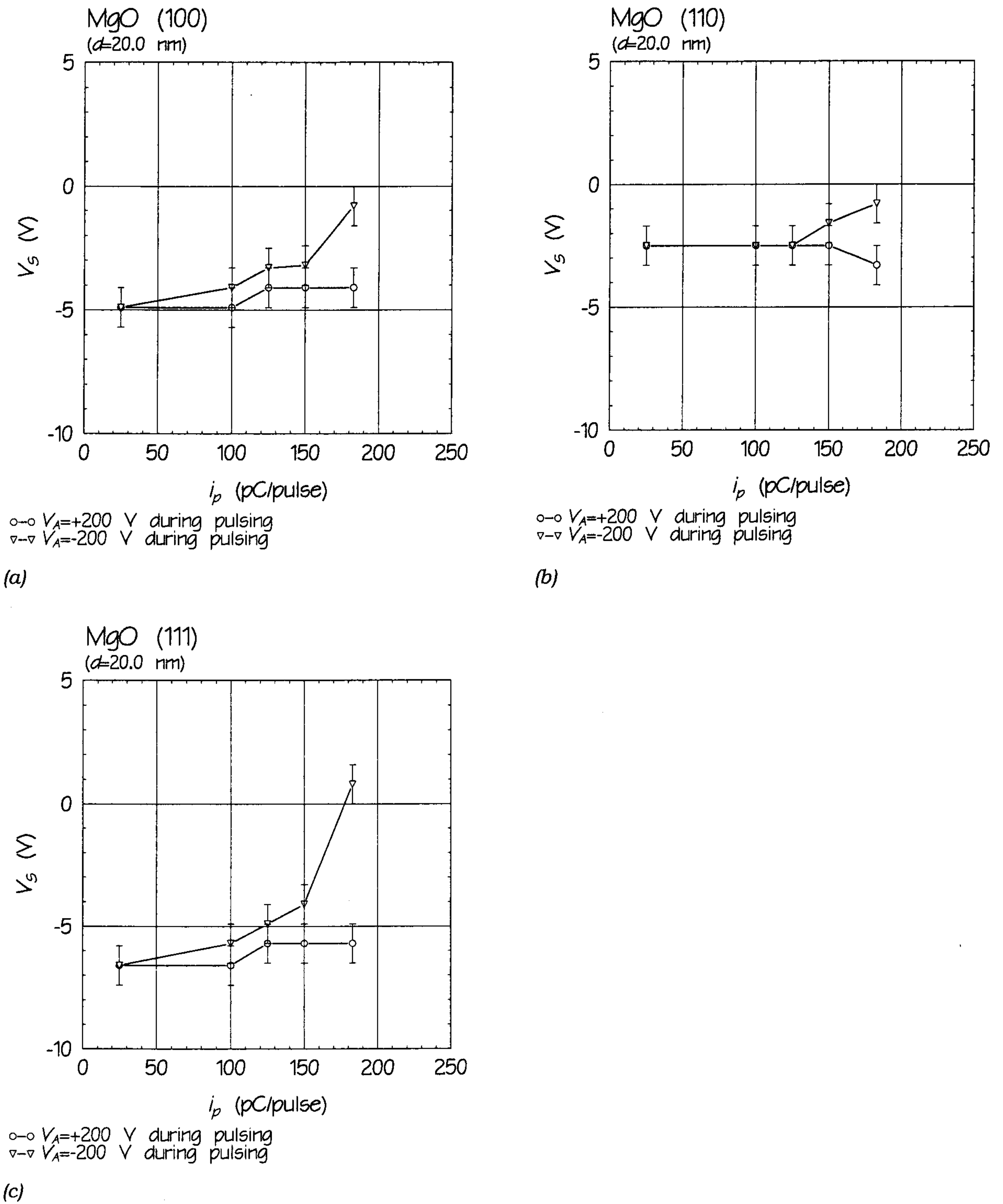

-Figure 4.19- *The induced surface potential as a function of i_p for samples with a different crystal face. The experiment was done with R=0.15 ± 0.05 mm and E_{gun}=1000 eV.*

Although there was no significant difference measured in the values of δ of the three MgO samples, a difference in charging properties is observed. The surface potential is most negative for the MgO (111) film and least negative for the MgO

(110) surface. Apparently the charging mechanism is influenced by the crystal orientation.

The last measurements of which the results are given are those on the MgO films grown upon n- and p-doped Si (Figure 4.20). The charge in n-Si is mainly carried by electrons and in p-Si mainly by holes. A difference may therefore be observed in the charging properties between MgO films grown upon these substrates.

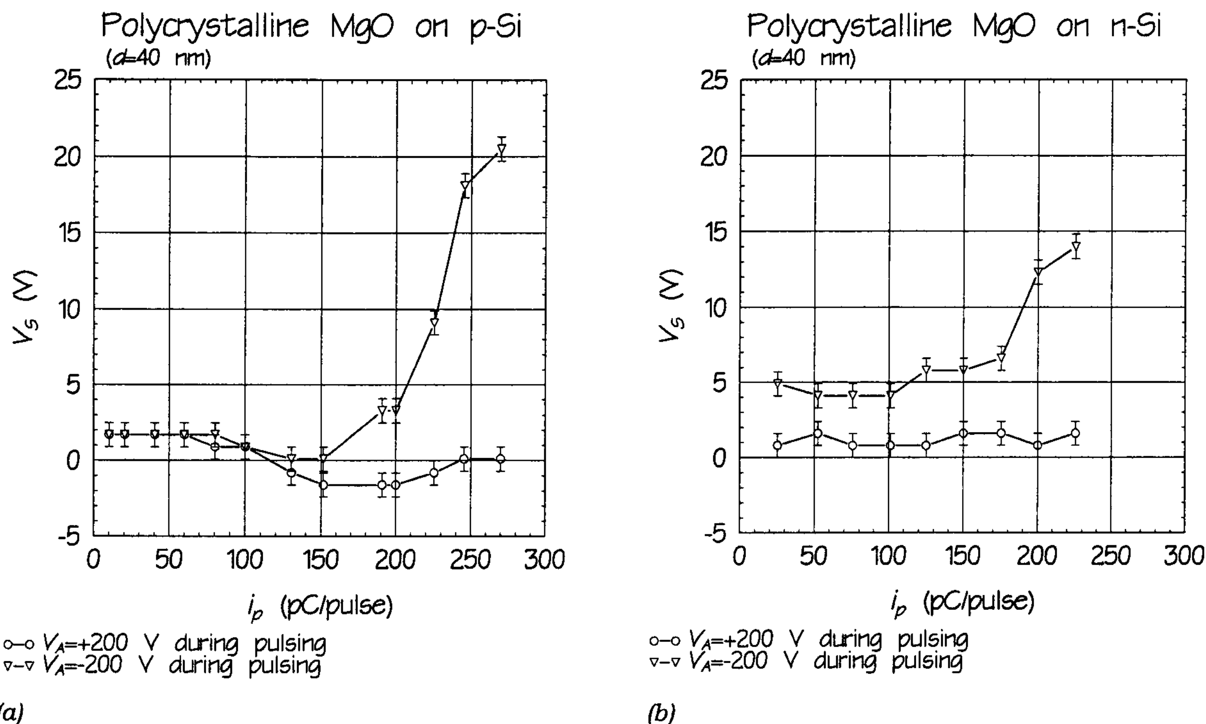

***Figure 4.20**- The induced surface potential as a function of i_p for a MgO films on a p-Si substrate (a) and a n-Si substrate (b). Beam radius R=0.15 ± 0.05 mm and E_{gun}=1000 eV.*

In contrast with the other measurements, in which V_S was negative for small values of i_p, a positive surface potential is induced at low primary currents. Comparing the results with those of the polycrystalline MgO grown on Fe_3O_4 it can be concluded that the charging mechanism is strongly influenced by the conductivity of the substrate. It is noted however that the effects may be enhanced by the thin insulating SiO_2 layer ($d \approx 2$ nm) between the MgO film and the Si substrate.
The MgO films grown directly on n- and p-Si, showed much more decay of the δ-curve than the mono- and polycrystalline samples grown on Fe_3O_4 (§4.1). It is possible that in case of MgO on Si the electrons are pulled back directly by a positive core potential than by the surface potential barrier caused by the inhomogeneity of the surface potential distribution. In what way the substrate influences the built up of charge, is difficult to say.
There is a difference of roughly 4 V between the induced surface potentials at $i_p \lesssim 160$ pC/pulse in figure 4.20(b), while in figure 4.20(a) no difference is observed for low values of i_p. So in case of V_A <0 V d.p. on the MgO film on n-Si a more positive surface potential is induced compared with the MgO film on p-Si. This is in agreement with observations during the measurements of δ of the two samples,

during which V_A is also negative. The δ-curve of MgO on n-Si decayed more than the δ-curve of MgO on p-Si.
According to Dresner [18] the current through the MgO is mostly carried by electrons. Therefore one would expect that the MgO on n-Si shows a behaviour of the surface potential, more comparable to that of MgO on a conducting substrate than the MgO on p-Si. The opposite is observed however. Maybe the reasoning is too simple. Important however is that it proves that the established surface potential distribution is influenced by the conductivity of the substrate.
The i_p beyond which V_S starts to rise, is comparable to the values found for the other samples of the same thickness. This indicates that the mechanism which induces the surface potential distribution is the same as for the other samples. Apparently only another equilibrium distribution is formed. The difference between the core potential in the two pulsing modes at high values of i_p is approximately 10 V for MgO grown on n-Si and approximately 20 V for MgO grown on p-Si. It was assumed before that at these high currents the charging mechanism for V_A=-200 V behaves more as expected from a homogeneously charged surface. In that case the dynamical equilibrium state may be less complex. Therefore the conclusion of Dresner, that the current through the MgO is mostly carried by electrons, may be used now to explain the higher surface charge of MgO on p-Si. The surface charge is less neutralized by electrons from the substrate, because in p-Si there are less electrons in the conduction band.

Subtle quantitative differences between the induced core potentials are observed on the MgO films grown on Fe_3O_4. They depend on the the electron beam radius, crystallinity, crystal orientation and sample thickness. However measurements on MgO films grown on n- and p-Si showed a strong dependence on the conductivity of the used substrate. A quantitative interpretation of the charging effects of insulating films and therefore an explanation how the core potential is influenced by the different parameters is a very complex occupation. One has to deal with complex charge distributions on the surface and within the interior of the film, caused by dynamical processes in which trajectories of new arriving charges are influenced by the field established previously by the former charges. Not only the processes on the surface, which are described by the calculations of Ying and Hendriks, but also processes in the interior of the film are of importance. For example according to Cazaux [14],[19] secondary electrons generated at a certain depth in the interior of the film can be trapped near the surface by the attraction by their electric images in the material and by defects at the surface caused by surface contamination. Therefore knowing the core potential under certain experimental conditions is not enough to understand the charging phenomenon quantitatively.
On the other hand the qualitative behaviour of the induced V_S looks the same in all measurements. For low values of i_p, a saturated core potential is established independent of V_A d.p.. This can be explained by the mechanisms described by Hendriks [15] and Ying [16]. For currents beyond a certain value, the potential induced with V_A <0 V d.p. starts to rise and reaches a new saturation value. The reason for this is not clear, but it is assumed that at these high currents the mechanism mentioned above breaks down and the core potential behaves more as expected from the sign of δ.

§4.4 SEE Enhancement

It was observed that when doing two successive SEE measurements on MgO, the δ_{max} of the second measurement was always higher than that of the first measurement. This was in contradiction with the experiments of Schmitz [17]. He found a decrease in $\delta(E_p)$ after successive measurements. The effect was caused by positive charging relative to V_A during the preceding measurements, which creates a potential barrier near the surface. This effect was already discussed in §2.2.

To study the enhancement of δ_{max}, the following experiment was devised. At first i_p was measured. With this calibration the δ-curves were measured. The sample was then pulsed for one minute with V_A =+200 V to establish a certain charge distribution in the sample. Note that this is in fact the same as what is done during a measurement of the primary beam current (§3.1), only far more pulses are given and V_A is higher. After that, five successive δ-curve measurements were done, giving five values of δ_{max}. Then the sample was pulsed with V_A=-200 V for one minute and after that again five δ-curves were measured. Note that pulsing with V_A =-200 V is in fact the same as what happens during the measurement of a δ-curve, in which the sample is also bombarded with electrons while V_A<0 V.
To check the reproducability of the measurements the procedure was repeated. So at the end of the experiment, 20 values of δ_{max} are obtained.
The method of establishing the charge distribution is similar to the method described in §4.3.

The result of such an experiment on the MgO(100) sample of the first batch is shown in figure 4.21.

When the surface is bombarded with V_A>0 V, a certain surface potential distribution is generated (figure 3.3). In the previous section it was pointed out that the negative ring surrounding the core acts as a potential barrier for the secondary electrons with their low kinetic energy. In §4.3 measurements of V_S as a function of i_p were done. It was shown that for the primary currents which are used here, no significant difference was found between the induced surface potential in the two pulsing modes. It was also mentioned that the only information the measurement of the onset of the δ-curve gives, is the value of the core potential. However in §4.2 it was concluded that qualitative information about the shape of the potential distribution can be obtained by studying the shape of the δ-curves at low energies. By doing this, it was observed that the δ-curves for E_p<E_I, obtained after the sample was pulsed with +200 V, were deeper than when the sample was pulsed with V_A=-200 V. So it seems that in the former case the surrounding ring is more negative than in the latter case, while the core potential is the same. This is visualised by the hypothetical curve in 3.3. It is possible that the potential barrier, induced with V_A =+200 V d.p., is higher than in case of V_A=-200 V d.p..

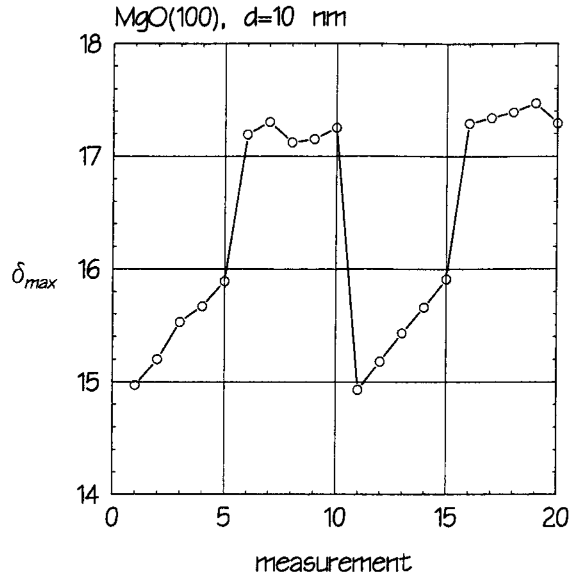

-**Figure 4.21**- *Studying the enhancement of δ after successive measurements. The measurements 1 to 5 and 11 to 15 were obtained after pulsing for one minute with V_A=+200 V, and the measurements 6-10 and 16-20 after pulsing with V_A =-200 V. The measurements were done with i_p=7.0 pC/pulse, R=2.0 ± 0.2 mm and E_{gun}= 1000 eV.*

From the foregoing, the behaviour of δ_{max} can then be interpreted in the following way.
The first measurement gives a low value of δ_{max}, because of the higher potential barrier, induced by the first pulsing procedure. A measurement of a δ-curve will lower this potential barrier, because during that measurement the sample is bombarded with V_A<0 V and therefore the surface potential is flattened. After the fifth measurement, the sample is pulsed with V_A=-200 V. The effect of flattening $V_S(r)$ is now accelerated due to the large amount of pulses with which the sample is bombarded and a certain saturation value is reached. The following measurements will not influence the surface potential anymore, because $V_S(r)$ is already as flat as as possible.
By then pulsing the sample again with V_A=+200 V, the initial surface potential is re-established.

In figure 4.22 the result is shown of the same experiment done on the wedge-shaped layer of the second batch. For higher film thicknesses it seems, that a saturation value is already reached after five measurements. Apparently the surface potential distribution is flattened more quickly. This may be caused by a worse charge drain to the substrate.
After pulsing with -200 V, δ_{max} decreases to the value, which is almost equal to the saturation value which is reached in measurement 5. It seems that a certain relaxation effect occurs. It is strange that $V_S(r)$ would become less flat when more measurements are done. Moreover, in the preceding section the relaxation time of the surface potential was estimated to be longer than seven hours.

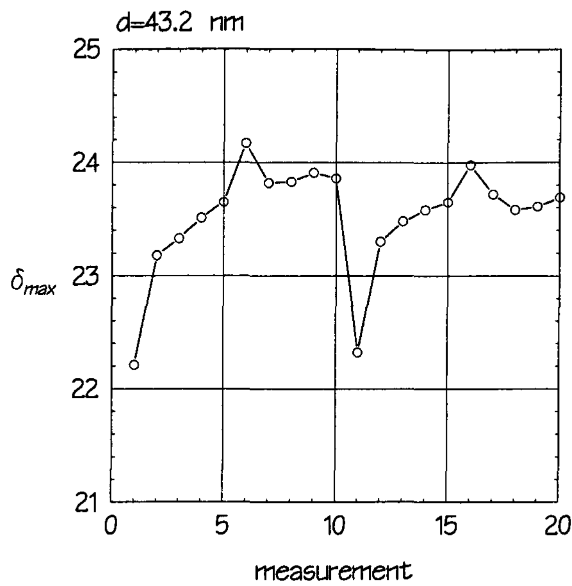

(a)

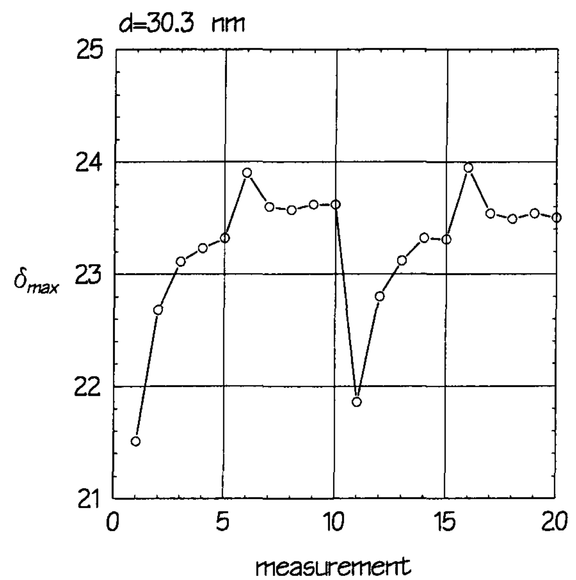

(b)

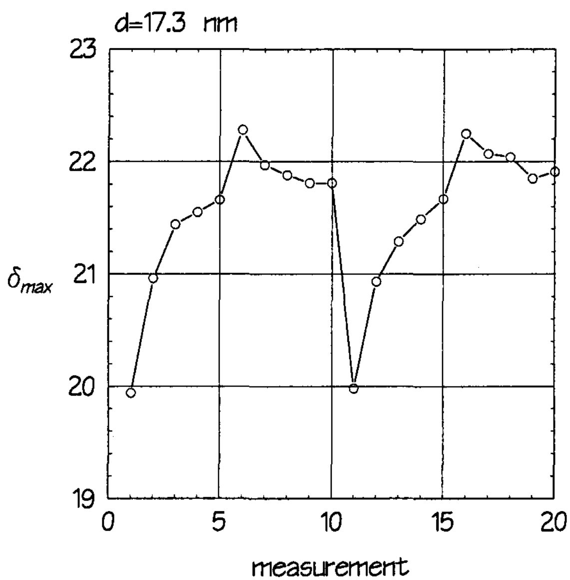

(c)

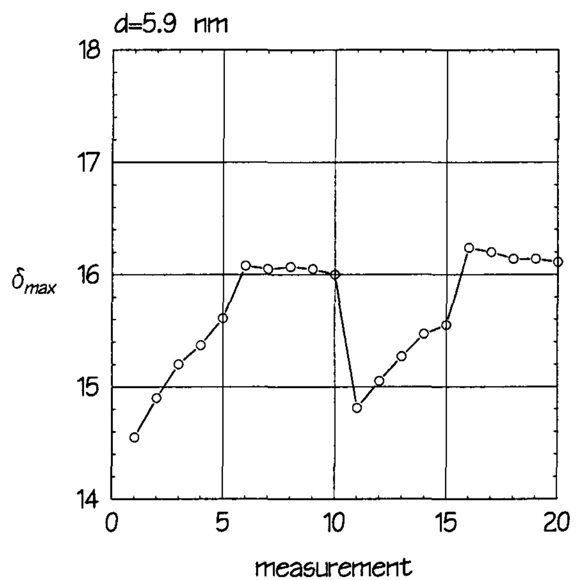

(d)

-Figure 4.22- *The enhancement of δ_{max} for different values of d. It seems that a certain relaxation effect occurs. For d=5.9 nm the relaxation time may be so short, that it cannot be observed. The measurements were done with i_p=7.0 pC/pulse, R=2.0 ± 0.2 mm and E_{gun}=1000 eV.*

In figure 4.23 the result is shown of an experiment for d=5.9 nm, but now with a primary beam current five times as high as in figure 4.22(d). It is clear that an increase of i_p has the same effect as an increase of the film thickness, which indicates that the difference between the measurements are indeed caused by a worse charge drain to the substrate.
It is also observed that all the measured values of δ_{max} are lower in case of i_p=35.0 pC/pulse than in case of i_p=7.0 pC/pulse. As mentioned in §2.2, a decreasing δ_{max} with higher beam current is caused by a higher potential barrier at the surface. But it is strange then, that the saturation value is also below the corresponding

value measured with low i_p. One would expect that when the surface potential is flattened, the difference between the measured values of δ_{max} would decrease, but this is not the case.

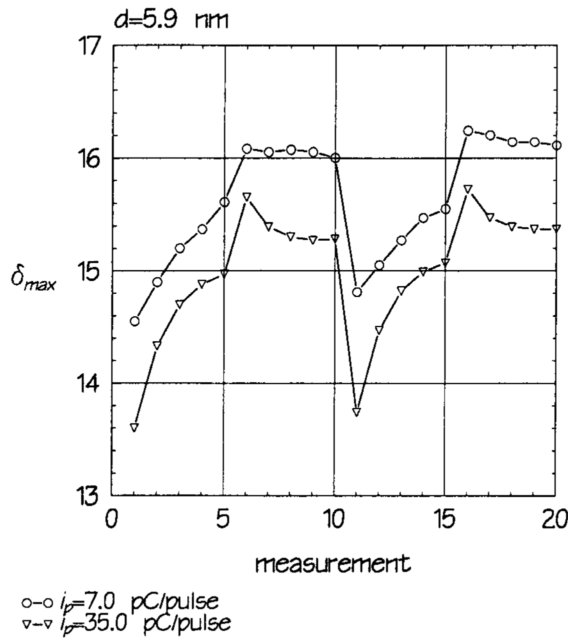

-Figure 4.23- *The enhancement of δ_{max} for d=5.9 nm and for two different values of i_p. It seems that an increase of i_p has the same effect as an increase of the film thickness. The relative enhancement seems to be higher for i_p=35.0 pC/pulse (21 % versus 11% for i_p=7.0 pC/pulse). R=2.0 ± 0.2 mm and E_{gun}= 1000 eV.*

It seems that it is difficult to give a consistent explanation of the observed effects in terms of the spatial distribution of the surface potential with the limited information about this surface potential distribution which is available for now.
On the other hand, the results of the measurements with higher i_p indicate, that the decrease of δ_{max} with increasing i_p and the increase of δ_{max} in successive measurements are to a certain extend independent effects. Besides the discrepancies which arise when the experiments are explained in terms of a change of $V_S(r)$, another argument for this is the fact that the relative effect of the increase of δ_{max} is greater for higher values of i_p, whereas the absolute values of δ_{max} decrease.

Another explanation of the increase of δ_{max} after successive measurements may be found in an effect known as secondary electron field enhancement (SEFE). Due to the strongly charging of the MgO film during electron bombardment a Fowler-Nordheim tunneling can occur of electrons from the conducting substrate, through the film, into the vacuum. The charging can also decrease the thermal excitation energy of trapped electrons, the so-called *Poole-Frenkel* effect (§2.1.1). Both effects can give an extra contribution to the secondary current.

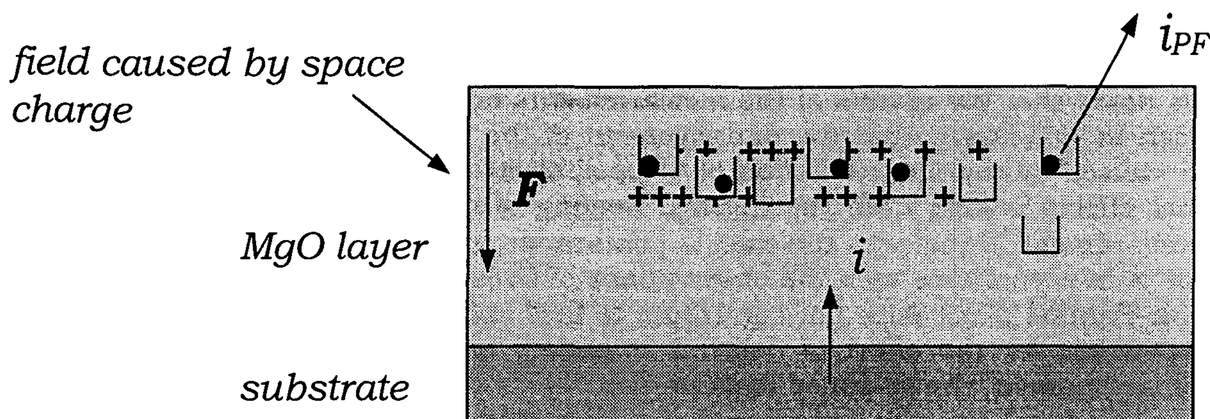

*-**Figure 4.24**- When δ>1 a positive space charge will be established. This will induce an electrical field in the film, which will rise until current continuity is established. If this field is sufficiently high (**O**(10^7 V/cm)), a fraction of the injected electrons will be emitted into the vacuum. This current thus represents a field enhanced component of the secondary emission. The electrical field also lowers the thermal excitation energy of trapped electrons, resulting in a Poole-Frenkel current i_{PF}.*

Note that a distinction is made between *space* charge and *surface* charge. The experimental result that a negative *surface* potential is found, when the sample is bombarded with electrons with $E_p>E_I$ does not exclude the possibility of SEFE. Because δ>1, the net charging of the sample will be positive. This positive space charge will determine the electrical field which is seen by the electrons in the substrate. The potential well, induced by the positive space charge may be so deep that the electrons can overcome the potential barrier at the surface.

The results can now be explained as follows. During pulsing with +200 V the mentioned surface potential is established. The withdrawal of the secondary electrons also minimizes the created internal field.
When a δ-curve is then measured a certain internal field is built up. A second measurement will increase this internal field and this results in a higher secondary emission. The internal field is maximized during pulsing with V_A=-200 V. When after one minute the pulsing is stopped, the internal field will relaxate. Even during a measurement of a δ-curve, the internal field will relaxate, because the repetition time of the pulses during a measurement of a δ-curve is much longer than 10 μs.
The greater relative increase of δ_{max} for higher values of i_p, can be explained by an increased internal field, through which a higher fraction of electrons is emitted into the vacuum.
It is assumed that the absolute decrease of the values of δ_{max} at higher primary currents is still caused by the inhomogeneous potential distribution at the surface. In this explanation it is assumed that the effect of SEFE is more or less independent of the effect caused by inhomogeneous potential distribution. This is not unlikely, because in section §4.3 it was shown that in both pulsing modes the magnitude of V_S was not changed, but more the spatial distribution. It is therefore possible that the changing surface potential hardly influences the effect of field

enhanced emission. The enhancement of δ_{max}, which is in all cases 10 to 20 %, is typical for SEFE [20].

It is noted that the results of the measurements are fully reproducable. From this it can be concluded that the enhancement of the secondary electron emission is not caused by thermal excitation of trapped electrons, the Poole-Frenkel effect, or other effects arising from the thermal heating of the sample due to the electron bombardment. If this was the case, a continuous increase of δ would be observed. This is in accordance with the observations of Dresner [18]. He concludes that the Poole-Frenkel effect does not contribute to field enhanced emission, but is mainly responsible for the effect of delayed secondary emission after switching off the primary current, the so-called *Malter effect*.
The reproducability also proves that the state reached in the two pulsing modes is independent of the state of the sample, before the pulsing was started.

It is noted that an *externally* applied electrical field can also influence the SEE, by changing the surface barrier of the material under consideration. This change of the surface barrier allows the electrons to tunnel from the solid into the vacuum. Notice that the external electrical field during the measurement of a δ-curve is not zero (Figure 3.1) and moreover not constant, because of the varying anode potential V_A. This external electrical field may cause an unintentional enhancement of the SEE of the film under consideration. It is shown however by Dresner [18] that the magnitude of electrical fields which cause a significant enhancement of the SEE is of the order of 10^7 V/cm. The external fields which are present above the sample during a SEE measurement are of the order of 10^3 V/cm, which is orders of magnitude too small to influence the SEE significantly.

As mentioned before the increase of δ in successive measurements was in contradiction with the experiments of Schmitz [17]. He found a decrease in $\delta(E_p)$ after successive measurements. It is noted that the MgO films he studied, were all grown on Si and glass substrates. Moreover the films were much thicker (140-230 nm). It has been observed in this work and by Schmitz, that the effects caused by an inhomogeneous surface potential distribution increase when the substrate is less conducting and when the sample is thicker. This effect may therefore dominate the SEFE effect under certain conditions. By studying the dependence of δ on i_p of a 230 nm MgO layer on Si, Schmitz found a decreasing δ with increasing i_p, in correspondence with an increasing surface potential barier. For $i_p \gtrsim 200$ pC/pulse however, δ was found to increase, for which no explanation was given. From the considerations above, an explanation may be that at these currents the internal field becomes so high that the SEFE effect starts to dominate.

Chapter 5: Conclusions

With the built experimental set-up it is possible to do measurements of the secondary electron emission yield of metals and insulators with primary energies up to 3400 eV. It is also suitable for doing LEED and AES, although the signal to noise ratio of the latter analysis technique is low. This is however intrinsic to the measuring method.
Depending on the lens voltages of the used electron gun, in some cases a polyenergetic electron beam is generated. Although this artefact could be avoided by choosing the right lens voltages, it is worthwile to study the possibility of replacing the electron gun.

The measurements were done on in all twelve samples, grown in six batches. The SEE properties of the samples of the last three batches differed from those of the other samples. With XPS, these differences could be imputed to a surplus of oxygen in the film, possibly due to a the presence of $Mg(OH)_2$ within the compound. The films of one batch differed in the SEE properties from all other samples. The reason for this could not be found with the used analytical techniques (AES, LEED, RBS and XPS). In the future work has to be done, to improve the reproducability of the MgO films.

It was found that the maximum secondary electron yield of monocrystalline MgO is higher than that of polycrystalline MgO. For monocrystalline MgO $\delta_{max}\approx 24$ and for polycrystalline MgO a δ_{max} of 16 was found. The SEE properties as a function of the film thickness were studied using wedge-shaped layers. For both mono- and polycrystalline samples it was found that beyond a certain film thickness, δ_{max} reaches a saturation value. The film thickness beyond which δ_{max} saturates is a measure for the secondary electron escape depth. For polycrystalline MgO this escape depth was found to be 20 nm, while for monocrystalline MgO (100) this escape depth was estimated to be 75 nm. The greater secondary electron escape depth in monocrystalline MgO explains the higher δ_{max} in comparison with polycrystalline MgO.
The values of δ_{max} and the escape depth were measured with the unmodified set-up, with which it was possible to do measurements of δ up to 1000 eV. Measurements of δ up to 3500 eV were done on other samples, but the results of these samples were less reliable, because of their high O/Mg ratio. For polycrystalline MgO it was found that $E_{max}\approx 1150$ eV, and for monocrystalline $E_{max}\approx 1350$ eV. This means that the values for δ_{max}, which were given above, are probably underestimated. Therefore, it is worthwile to repeat the experiment with the wedge-shaped layers in the future, with more reliable MgO films. The escape depth of 75 nm for monocrystalline MgO was obtained by extrapolation. To obtain a more accurate value of the escape depth, a wedge-shaped layer thicker than 50 nm has to be grown in the future.
The lower δ_{max} for polycrystalline MgO cannot be explained by a possible lower δ_{max} of MgO(111) and MgO(110), because no influence of the crystal orientation on δ_{max} was found.

Measurements of δ_{max} on MgO films grown on n- and p-Si substrates showed no measurable influence of the different electronic structure of the substrates, for film thicknesses down to 5 nm.

For both mono- and polycrystalline MgO, an E_I of 15 eV was found and for film thicknesses down to 5 nm, no influence of the film thickness on the value of the first cross-over energy was observed. The reason is that at these primary energies, for both mono- and polycrystalline MgO, the penetration depth of the primary electrons is much lower than the secondary electron escape depth. From these results it can also be concluded that as far as the SEE properties are concerned, the film thickness, below which the electronic structure of MgO starts to differ from the electronic band structure of bulk MgO is smaller than 5 nm, which is equivalent to 12 monolayers.
No significant dependence on the crystal orientation nor on the substrate was found.

From numerical simulations it was found, that the typical features, which are observed on the δ-curves of insulating samples for $E_p \leq E_I$, are caused by an inhomogeneous surface potential distribution. This potential distribution is probably formed during the measurement of i_p, preceding a measurement of a δ-curve.
This result can be used in the future to study the surface potential distribution. A possible experiment is the following. With certain values for V_A, E_{gun} and R a surface potential distribution is established by pulsing for a certain time span. Then a δ-curve is measured with a beam radius. After that, the initial surface potential distribution is re-established. Then another δ-curve is measured, but now with another value of R. By repeating this procedure for various values of R, and after deconvoluating the obtained δ-curves a potential distribution can be obtained. Although the reliability of this potential distribution depends fully on the reliability of the used model to deconvoluate the shape of the potential distribution from the E_I-curves, the result can be useful in the explanation of other observed effects, in which the surface potential distribution is assumed to play a role.
The strong influence of a defocussing of the electron beam on the shape of the δ-curves at low primary energies, which was also found from the numerical simulations, is hardly observed in practice. This is probably caused by an overestimation of the divergence of the electron beam in the simulations. This can be verified by a quantitative analysis of the divergence of the electron beam, which should be done in the future.
In order to measure the intrinsic δ-curve at low primary energies as good as possible, the beam current should be measured in another way, for example by using a Faraday cup. Another method is to discharge the sample between the measurement of i_p and of the δ-curve. This can be done by heating the sample or by spraying the sample with low energetic electrons using a so-called *flood gun*. The latter method seems to be the most favourable, because it gives the least extension of the time span of a measurement of $\delta(E_p)$.

The qualitative behaviour of the core potential induced by electron bombardment, with V_A=+200 V and -200 V during pulsing, looks the same for all samples. For low values of i_p, a saturated core potential is established independent of the sign of V_A during pulsing. This can be explained by the mechanisms described by Hendriks

[15] and Ying [16]. For currents beyond a certain value, the potential induced with V_A=-200 V d.p. starts to rise and reaches a new saturation value. It is assumed that at these currents the first mechanism breaks down and that the surface potential distribution behaves more as expected from the sign of δ. This means that the surface potential flattens when the surface is bombarded with electrons while V_A <0 V, in comparison with the surface potential induced with V_A >0 V during pulsing. This is in agreement with the interpretation of the shape of the E_1 curves.

For low values of i_p, the MgO films grown on Si are the only samples on which *positive* values of the core potential are found. This corresponds with the severe charging effects observed during measurements of $\delta(E_p)$ of these samples. Apparently the induced surface potential depends strongly on the conductivity of the substrate.

The only direct information about the surface potential distribution which was obtained in this work, is the value of the core potential. This makes a *quantitative* interpretation of the charging effects of insulating films and therefore an explanation how the potential distribution is influenced by different parameters very complex.

In order to study the charging phenomena more quantitatively in the future, more information about the spot profile is needed. This information can be obtained by doing SEE measurements on a sample, consisting of a metal substrate which is covered half by a another metal differing in the SEE properties. By the interpretation of the change in δ, while moving the electron beam across the edge of the step, information about the spot profile can possibly be obtained. Another method uses a so-called Faraday cup. By moving the electron beam across the opening of the Faraday cup and measuring the absorbed current, information of the spot profile can be obtained.

The most consistent explanation of the observed increase of the SEE of MgO in successive measurements, is secondary electron field enhancement.

It is assumed that the enhancement of the measured δ in successive measurements is caused by a space charge, induced by the electron bombardment in the interior of the film under consideration. This space charge establishes a Fowler-Nordheim tunneling of electrons through the substrate-MgO interface. When the internal field is high enough, a part of these electrons can be emitted to the vacuum, giving a field enhanced contribution to the secondary current.

In this explanation the electronic band structure of the substrate determines the magnitude of the effect. Therefore in the future the influence of the substrate on the enhancement of the SEE has to be studied.

References

[1] L. AUSTIN, H. STARKE; *Über die Reflexion der Kathodenstrahlen und eine damit verbundene neue Erscheining sekundärer Emission*, Ann.Phys. Lpz., **9**, p 271, 1902.

[2] R.G. LYE, Phys. Rev., **99**, p 1947, 1955.

[3] N.R. WHETTEN, A.B. LAPONSKY; J. Appl. Phys., **30**, p 432, 1959.

[4] M.BRONSHTEYN, A.N. BROZDNICHENKO; *Inelastic Scattering of Electrons and Secondary Electron Emission of Magnesium and Magnesium Oxide*, Radio Eng. Electron. Phys., **15**, No. 8, p 1474, 1970.

[5] V.L. BORISOV, V.N. LEPESHINSKAYA; *Methods for increasing the efficiency of magnesium oxide secondary emitters*, Bulletin of the Academy of Sciences of the USSR, Physical Series, **40**, no. 8, p 83, 1976.

[6] H. BRUINING, *Physics and Applications of Secondary Electron Emission* (Pergamon Press, London, 1954).

[7] J.P. GANACHAUD, A. MOKRANI, *Theoretical study of the secondary electron emission of insulating targets*, Surface Sci., **334**, p 329, 1995.

[8] D.C. JOY, *A model for calculating secondary and backscattered electron yields*, J. Microsc., **147**, p 51, 1987.

[9] R.E. THOMAS, A. SHIH, G.A. HAAS; *Electron energy loss and secondary emission in BaO*, Surface Sci., **75**, p 239, 1978.

[10] G.F. DIONNE, *Effects of secondary electron scattering on secondary emission yield curves*, J. Appl. Phys., **44**, p 5361, 1973.

[11] G.F. DIONNE, *Origin of secondary-electron-emission yield-curve parameters*, J. Appl. Phys., **46**, p 3347, 1975.

[12] R. MARTINELLI, Appl. Phys. Lett., **17**, p 313, 1970.

[13] H. VON SEGGERN, *Charging dynamics of dielectrics irradiated by low energy electrons*, IEEE Trans. Nuc. Sci., **NC-32**, 1985.

[14] J. CAZAUX, K.H. KIM, O. JBARA, G. SALACE; *Charging effects of MgO under electron bombardment and nonohmic behaviour of the induced specimen current*, J. Appl. Phys., **70**, p 960, 1991.

[15] J.J. SCHOLTZ, R.W.A.H. SCHMITZ, B.H.W. HENDRIKS, S.T. DE ZWART; *Influence of charging on secondary electron yield measurements*, Nat. Lab. Report 6801, 1994.

[16] M.H. YING, J.T.L. THONG; *Insulator charging under irradiation with a stationary electron probe*, Meas. Sci. Technol., **5**, p 1089, 1994.

[17] R.W.A.H. SCHMITZ, *Secundaire electronen emissie*, Thesis, Techn. Univ. Eindhoven, 1995.

[18] J. DRESNER, *Delayed secondary-electron emission in thin MgO layers*, J. Appl. Phys., **48**, p 4760, 1977.

[19] J. CAZAUX, *Electrostatics of insulators charged by incident electron beams*, J. Microsc. Spectrosc. Electron., **11**, p 293, 1986.

[20] H.-J. FITTING, *Secondary Electron Field Emission*, Phys. Stat. Sol. (a), **108**, p 265, 1988.

Dankwoord

Ter afsluiting wil ik nog een aantal mensen noemen die een bijdrage hebben geleverd aan dit afstudeerwerk.
Allereerst wil ik mijn afstudeerbegeleider Hans Scholtz bedanken voor de prettige samenwerking tijdens mijn stage. Met zijn nuttige adviezen, het corrigeren van het verslag, de numerieke simulaties die hij deed en met zijn niet aflatend enthousiasme heeft hij een aanzienlijk aandeel gehad in het slagen van de stage. Onze discussies leidden vaak tot een beter inzicht in de bestudeerde materie en in andere zaken.
Dit laatste geldt ook voor Gerke Jaarsma, met wie ik ook prettig samen heb gewerkt.
Verder wil ik ook de mensen van de vacuümdienst en van de elektronica ontwerpgroep bedanken, die mij geholpen hebben bij het oplossen van de problemen die zich voordeden bij het bouwen van de opstelling.
Ook de mensen van XPS, SIMS en RBS hebben door hun analyses van de preparaten hun bijdrage geleverd.
Ronald Wolf, Pascal Bloemen, Jim Gaines en Johan van Eemeren wil ik bedanken voor het groeien van de MgO lagen en voor de prettige samenwerking gedurende de tijd dat we op elkaars lip hebben gewerkt.
Als laatste wil ik Prof. Brongersma van de TUE en Philips bedanken voor het mogelijk maken van deze stage op het Nat.Lab..

Eindhoven, 7 december 1995.

Appendix: MgO Data Table

Molecular weight:	40.32	
Physical Density:	3.576 g/cm^3	
Mineral Name:	periclase	
Color:	colorless and transparent	
Cleavage:	(100) perfect	
Crystal Structure:	cubic (fcc)	
Lattice Constant:	0.42120 ± 0.00003 nm	(T=293 K)
	0.42758 nm	(T=1373 K)
Melting Point:	3125 K	
Dielectric Constant:	9.8 (static)	(T=300 K)
Electrical Resistivity:	$1.3 \cdot 10^{15}$ Ωcm^{-1}	(T=573 K)
	$2 \cdot 10^{7}$ Ωcm^{-1}	(T=1273 K)
Mobility:	10 cm^2/Vs	
Energy Gap:	7.77 ± 0.01 eV	(T=295 K)
Electron Affinity:	0.85 eV	
Work Function:	3.55 eV	(T=1102-1182 K)
Magnetic Susceptibility:	$-0.25 \cdot 10^{-6}$ cgs	
Index of Refraction:	1.741	(T=293 K)

Data taken from: M. Neuberger, D.B. Carter; *Magnesium Oxide*, Hughes Aircraft Company (Electronic Properies Information Center), **DS-163**, 1969

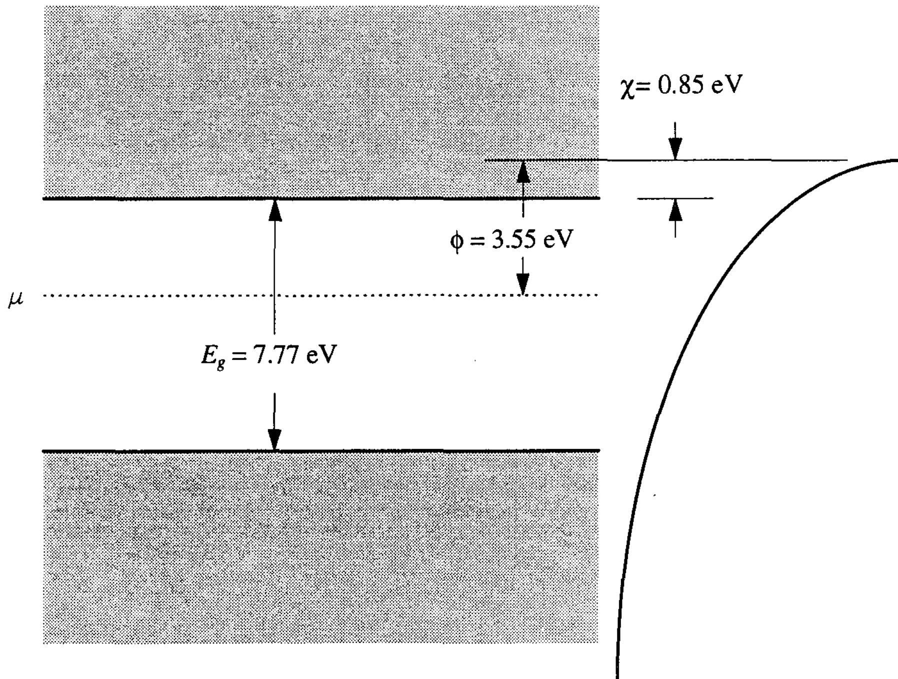

Figure A1- *Band picture of MgO.*